A PHYSICAL CHANNEL MODEL AND ANALYSIS OF NANOSCALE NEURO-SPIKE COMMUNICATION

A THESIS SUBMITTED TO
THE GRADUATE SCHOOL OF NATURAL AND APPLIED SCIENCES
OF
MIDDLE EAST TECHNICAL UNIVERSITY

BY

EREN BALEVİ

IN PARTIAL FULFILLMENT OF THE REQUIREMENTS
FOR
THE DEGREE OF MASTER OF SCIENCE
IN
ELECTRICAL AND ELECTRONICS ENGINEERING

AUGUST 2010

Approval of the thesis:

A PHYSICAL CHANNEL MODEL AND ANALYSIS OF NANOSCALE NEURO-SPIKE COMMUNICATION

submitted by **EREN BALEVİ** in partial fulfillment of the requirements for the degree of **Master of Science in Electrical and Electronics Engineering Department, Middle East Technical University** by,

Prof. Dr. Canan Özgen
Dean, Graduate School of **Natural and Applied Sciences** _____

Prof. Dr. İsmet Erkmen
Head of Department, **Electrical and Electronics Engineering** _____

Assoc. Prof. Dr. Özgür Barış Akan
Supervisor, **Electrical and Electronics Engineering Dept., METU** _____

Examining Committee Members:

Prof. Dr. Buyurman Baykal
Electrical and Electronics Engineering Dept., METU _____

Assoc. Prof. Dr. Özgür Barış Akan
Electrical and Electronics Engineering Dept., METU _____

Assoc. Prof. Dr. Ali Özgür Yılmaz
Electrical and Electronics Engineering Dept., METU _____

Asst. Prof. Dr. Asaf Behzat Şahin
Electrical and Electronics Engineering Dept., METU _____

Metin Aktaş
ASELSAN, M.Sc. _____

Date: _____

I hereby declare that all information in this document has been obtained and presented in accordance with academic rules and ethical conduct. I also declare that, as required by these rules and conduct, I have fully cited and referenced all material and results that are not original to this work.

Name, Last Name: EREN BALEVİ

Signature :

ABSTRACT

A PHYSICAL CHANNEL MODEL AND ANALYSIS OF NANOSCALE NEURO-SPIKE COMMUNICATION

Balevi, Eren
M.Sc., Department of Electrical and Electronics Engineering
Supervisor : Assoc. Prof. Dr. Özgür Barış Akan

August 2010, 60 pages

Nanoscale communication is appealing domain in nanotechnology. There are many existing nanoscale communication methods. In addition to these, novel techniques can be derived depending on the naturally existing phenomena such as molecular communication. It uses molecules as an information carrier such as molecular motors, pheromones and neurotransmitters for neuro-spike communication. Among them, neuro-spike communication is a vastly unexplored area. The ultimate goal of this thesis is to accurately investigate it by obtaining a realistic physical channel model. This model can be exploited in different disciplines. Furthermore, the model can help designing novel artificial nanoscale communication paradigms. The modeled channel is analyzed regarding the error probability of detecting spikes depending on channel parameters. Moreover, channel delay is characterized and information theoretical analysis of packet release mechanism in the channel is performed.

The modeled channel is extended to multi-input single output terminal. In this case, input neurons can simultaneously send information through the same synapse lead-

ing to interference. However, there is an interference repressing technique in these synapses called automatic gain control. It decreases the interference level observed on weaker signal. The first aim for this case is to define the interference channel at synapse having automatic gain control. The second aim is to analyze the achievable rate region of this channel. The analysis shows that gain control mechanism prevents the decrease in achievable rate region because of the weaker signal. Moreover, power, firing rate and number of stronger inputs do not affect the achievable rate region.

Keywords: Nanoscale communication, neuro-spike communication, physical channel model, gaussian interference channel, achievable rate

ÖZ

NANO ÖLÇEKLİ NÖRO-SPAYK HABERLEŞMENİN FİZİKSEL KANAL MODELLEMESİ VE ANALİZİ

Balevi, Eren
Yüksek Lisans, Elektrik Elektronik Mühendisliği Bölümü
Tez Yöneticisi : Doç. Dr. Özgür Barış Akan

Ağustos 2010, 60 sayfa

Nano ölçekli haberleşme, nanoteknoloji için ilgi çekici bir alandır. Nano ölçekli haberleşme amaçlı kullanılan birçok method vardır. Bunlara ilaveten, doğada bulunan haberleşme fenomenlerinden yeni nano ölçekli haberleşme teknikleri türetilebilir. Bunlardan biri moleküler haberleşmedir ve bu haberleşme tekniğinde bilgi taşıyıcı olarak moleküller, örneğin moleküler motorlar, feromonlar ve nöro-spayk haberleşme için nörotransmitter maddeler kullanılır. Bunlardan nöro-spayk haberleşme henüz keşfedilmemiş bir alandır. Bu tezin asıl amacı nano ölçekli nöro-spayk haberleşmeyi tam olarak incelemek için gerçekçi bir fiziksel kanal modelini elde etmektir. Bu model farklı alanlarda da kullanılabilecektir. İlaveten, bu model yeni yapay nano ölçekli haberleşme paradigmaları türetmekte yardımcı olabilir. Bu çalışmada modellenen kanal, kanal parametrelerine bağlı olarak spaykları tespit etmedeki hata olasılığı ve kanaldaki gecikme açısından analiz edilmektedir. Ayrıca, kanalın paket salgılama yapısı için bilgi kuramsal analiz yapılacaktır.

Modellenen kanal multi-input ve tek output olarak genişletilebilir. Bu durumda, input

nöronlar aynı zamanda aynı sinaps üzerinden gönderim yapabilir. Bu da girişime neden olur. Fakat bu sinapslarda girişim önleyici otomatik kazanç kontrol sistemi vardır. Bu sistem zayıf sinyal üzerindeki girişimi, sinyalin sinaptik katsayısını arttırarak azaltır. Bunun için ilk amaç, sinapslarda bu kontrol sistemine sahip bir girişim kanalı tanımlamaktır. Bu durum için ikinci amaçsa kanalın erişilebilir değer alanını analiz etmektir. Yapılan analiz, otomatik kazanç kontrol sisteminin, zayıf sinyale bağlı erişilebilir değer alanının düşmesini önlediğini göstermektedir. Ayrıca, kuvvetli sinyallerin gücünün, spayk oluşma oranının ya da sayısının artması erişilebilir değer alanını değiştirmemektedir.

Anahtar Kelimeler: Nano ölçekli haberleşme, nöro-spayk haberleşme, fiziksel kanal modeli, gauss dağılımlı girişim kanalı, erişilebilir değer

To my family

ACKNOWLEDGMENTS

I would like to express my deepest gratitude and respect to my advisor, Dr. Özgür B. Akan for his continuous support. His encouragement always motivated me throughout the research.

I would like to thank ASELSAN Inc. for the facilities provided during my M.Sc. degree. I am also grateful to TUBİTAK for its financial support to scientific research.

Finally, I would like to pay my sincere thanks to my family for their support, patience and faith to me in every aspect of life.

TABLE OF CONTENTS

LIST OF TABLES

TABLES

LIST OF FIGURES

FIGURES

CHAPTER 1

INTRODUCTION

The imagination of making more powerful things in a much smaller size creates the nanotechnology. It improves the current technology in almost every field as well as the human life. It is a rapidly growing area and its applications that comprise hundreds of nanodevices become more of an issue in each passing day. Therefore, communication between nanodevices turns out a critical theme. Hence, it is worthwhile to specify the communication paradigms for these tiny components in order to have a complete interaction among them.

1.1 Nanonetworks

Although nanodevices have limited capabilities, a group of them, which constitute the nanonetwork, can achieve complex tasks in a collaborative fashion. However, fundamental properties of nanonetworks differ than the classical ones in terms of their smaller size, lower resolution in sensing the environment, higher deployment density and low power consumption. These advantages can bring them many potential applications areas in [1]

- Immune system support
- Bio-hybrid implants
- Drug delivery systems
- Health monitoring

- Genetic engineering
- Food and water quality control
- Functionalized materials and fabrics
- Nuclear, biological and chemical (NBC) defenses
- Nano-functionalized equipments
- Biodegradation
- Animals and biodiversity control
- Air pollution control

Despite having many application areas, it does not exist many communication techniques that are appropriate for nanonetworks. Therefore, highly intelligent nanoscale communication paradigms are needed in order to provide a proper communication between them. At this point, novel nanoscale communication techniques are substantially valued.

1.2 Nanoscale Communication

Nanoscale communication has progressed parallel to the inventions in the nanotechnology. The communication via scaled down traditional electrical circuitry without touching its atomic properties is one representative of nanoscale communication. Unlike scaled down electronics components, atomic level properties are used in carbon nanotubes communication which is another instance of nanoscale communication. Carbon nanotubes have significant properties such as extremely high electrical conductivity, low power dissipation, allowing carriers to pass through the tubes with zero scattering and zero heat dissipation. These make them a special technique for communication purposes. Furthermore, the devices based on nanowires and quantum dots can be other examples of nanoscale communication.

In addition to these, the contributions of naturally existing phenomena can help to derive novel nanoscale communication methods. Molecular communication is the most

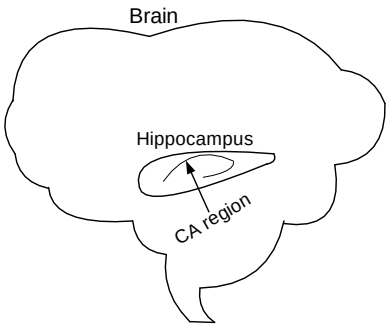

Figure 1.1: CA region in the hippocampus location of the brain.

promising one for this purpose. Although molecular communication is a completely new communication paradigm, it can be an efficient way for connections of nanomachines and used in nanonetworks [1], [14], [15]. Molecular communication is utilized in nanonetworks as three main architectures in terms of molecule propagation, which are walkway-based, flow-based and diffusion-based architectures [20].

The fundamental properties of the molecular communication are the encoding and decoding of the information via molecules, low transmission speed, low energy consumption and selective reception mechanism [16]. Moreover, in molecular communication, molecules are used as an information carrier such as molecular motors [8], pheromones and neurotransmitters [12]. Among them, neuro-spike communication that uses the neurotransmitters as an information carrier is a vastly unexplored communication paradigm.

Neuro-spike communication is based on the communication between neurons where the transmission is done by impulses and neurotransmitters. It is a hybrid communication model that includes both the electrical transmission of impulses and molecular communication due to neurotransmitters.

Neuro-spike communication may show some differences due to various types of neurons. Although neurons have different firing pattern of the cell, neurotransmitters type, receptors, the communication of neurons at CA region in the hippocampus location of the brain, shown in Figure 1.1, is chosen for modeling.

There are several reasons for selecting this location. The first one, the principal neurons at the CA are the place cells. Place cells are an example of the complex spike cell

such that they can both fire simple single spike and complex spike, i.e., the combination of two to seven individual spikes [23]. They have lower refractory period, that is, necessary time that passes to produce the next spike, and the smaller the refractory period, the more accurate the input information is represented. Moreover, the neurons in the hippocampus location are used frequently in neurophysiology, and hence, there exist many experimental results which can clarify their properties. Furthermore, hippocampus region is one of the most important part of the brain responsible for memory functions, thereby modeling the communication behavior of that part can be key factor for further investigations.

1.3 Related Work

In order to investigate the neuro-spike communication at CA region of hippocampus, the physiological principles of the CA neurons have to be known. In literature, there are several studies about them. The axonal propagation in the hippocampal CA3 neurons [19] and how reliable the axonal transmission occurs in this location are investigated [21]. In case of synaptic transmission, the vesicle release function of the hippocampal neurons is described [7], [26] related with the some synaptic concepts. The analysis of the vesicle release in hippocampal is further discussed [24]. Trial-to-trial variability in synapses is explained [2], [18] by making some experiments and interpreting their results.

Furthermore, a synaptic model pertaining to the neuro-spike communication is proposed [17]. It involves the fundamental events during the synaptic transmission, namely the vesicle release function of the neuron in response to a spike, excitation due to the vesicle release, called Excitatory Post Synaptic Potential (EPSP) and trial-to-trial variability of this potential. These phenomena are covered as different blocks in the model and then, analyzed information theoretically in terms of signal estimation and signal detection criteria with an appropriate encoding and decoding. The analysis results show that redundancy in neural communication improves the efficiency of transmitting the information when compared with single synapse in terms of reliability and robustness.

In neuro-spike communication, synapses are shared mediums leading to interference. The observation of achievable rate region of synaptic interference channel is a crucial problem.

In literature, the achievable rate region of channels shared by more than one input-output pair is heavily studied, particularly when the noise is Gaussian. The achievable rate region is obtained [31] when the interference level is very strong. Moreover, Sato [32] and Han-Kobayashi [33] furthered the approachable rate region for the strong interference level. In case of weak interference, it is stated that treating the weak interference as noise gives the best solution [31].

1.4 Motivation and Overview of This Work

The performance of neuro-spike communication is quite well in terms of reliability, speed and robustness. In this manner, realistic physical channel model of neuro-spike communication at CA region in the hippocampus location of the brain is substantially needed to be able to completely characterize its fundamental properties. Other disciplines such as neuroscience, medicine may benefit from the model in the future as well. Moreover, this model can be used to derive new nanoscale communication paradigms. To illustrate, using this channel for artificial nanonetworks produces a novel bio-inspired nanoscale communication technique.

Although there are many studies related with the physiological principles of the hippocampal neurons, none of these deal with the communication behaviors of neurons as a new nanoscale communication paradigm and model the end-to-end neural channel.

There is a synapse model in [17], however it does not cover the use dependent change of neurons or plasticity which is the change in the behavior of the channel from one usage to the other. Moreover, the diffusion of neurotransmitters in the synapse is not considered. Furthermore, the effect of different type receptors are not taken into account on EPSP generation. These shortcomings deviate the synaptic channel model from the realistic neural behavior.

The main objective of this thesis is to derive a realistic physical channel model of nanoscale neuro-spike communication between two terminals in terms of the communication theory basics. Here, realistic refers to coherent with physiological behaviors of neurons. For this purpose, first of all, neuro-spike communication is expressed by dividing it into basic building blocks. After that, each block is detailly investigated in order to model it with the basic communication subsystems. Eventually, the modeling of each neuro-spike basic block yields a complete channel model. In this work, the input-output analysis of the modeled channel is performed, and to reduce the uncertainty in the modeled channel behavior an information theoretical approach is introduced.

Though physical channel model is designed between one input and output terminal, it is extended to the many input, single output case to investigate the effect of interference in neuro-spike communication at CA region. For this case, there is an interference repressing technique in these synapses called automatic gain control, which decreases the interference level on the weaker signal by increasing its synaptic weight and increases its achievable rate region.

Although there are several studies about the achievable rate region for multi-user communication, none of these studies deal with the subject such that the interference level is altered by the channel according to the input strength.

The other objective is to define a special Synaptic Gaussian Interference Channel and to characterize its achievable rate region where the interference is adjusted by the channel automatically.

The remainder of this thesis is organized such that in Chapter 2, the fundamental principles of the neuro-spike communication at CA region is introduced and modeled. The complete physical channel model of neuro-spike communiation is given and its analysis is performed in Chapter 3. Numerical analysis of the channel is investigated in Chapter 4. Moreover, in Chapter 5, Synaptic Gaussian Interference Channel is defined and achievable rate region of this channel is analyzed. The thesis is concluded with Chapter 6.

CHAPTER 2

NEURO-SPIKE COMMUNICATION

Action potentials, i.e., spikes or impulses, are used while information is transmitted from one neuron to the other. Hence, it is called as neuro-spike communication. The neuro-spike communication between any input neuron and output neuron is shown in Figure 2.1.

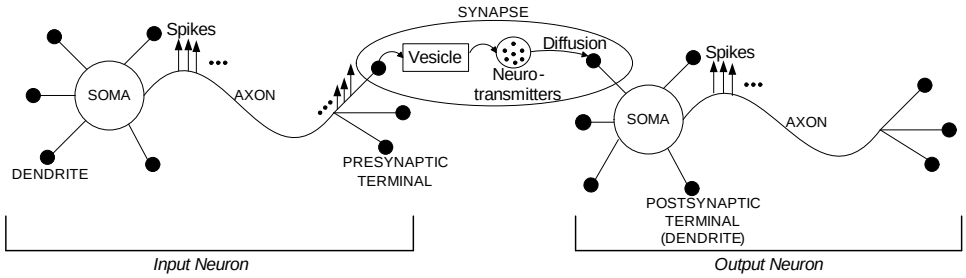

Figure 2.1: Neuro-spike communication.

It can be divided into three main parts:

1. *Axonal transmission*: The propagation of the spikes along the axon at the input neuron, which can be considered as wired communication.

2. *Synaptic transmission*: The release of neurotransmitters, diffusion of these neurotransmitters and the excitation on the output neuron due to them, which can be considered as wireless communication. Unlike the classical wireless communication methods, instead of an electromagnetic wave, neurotransmitter substances are used as a carrier in synaptic transmission.

3. *Spike generation*: Forming impulses at the output neuron provided that the excitation level exceeds the threshold value of the output neuron.

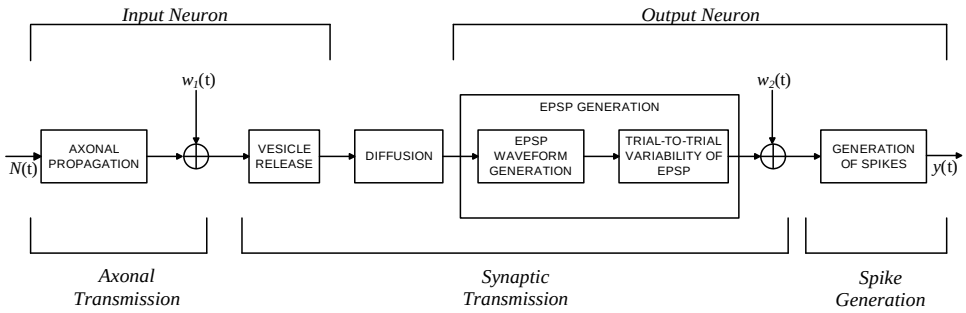

Figure 2.2: Block diagram of the neuro-spike communication.

One example of the neuro-spike communication is present at the CA region in the hippocampus location of the brain. The block diagram of the spike communication between single presynaptic terminal of the input neuron and single postsynaptic terminal of the output neuron at CA region is given in Figure 2.2.

The signals at the input are coded as spike trains denoted as $N(t)$ and propagate through the axon in the CA region of the hippocampus place cell. How reliable these trains are transmitted is explained in axonal propagation block.

In synaptic transmission, vesicle release, diffusion and EPSP generation blocks are included, respectively. Vesicle is released in response to a spike. This release occurs from the special terminals on the input neuron called *presynaptic terminal* or *synaptic bouton* to the synapse. After that, neurotransmitters, e.g., glutamate molecules for hippocampal neurons, are diffused through the synapse. They affect the specialized areas at the output neuron called *postsynaptic terminal* leading to the EPSP generation. EPSP generation block has two main functionalities. First one is the modulation of a single vesicle to an analog continuous signal and the second is the variability of this continuous signal.

The last block realizes the spike generation from the EPSPs where the output spikes are denoted as $y(t)$.

In case of noises, the system has two types of noise. These are the axonal noise, $w_1(t)$ and the synaptic noise, $w_2(t)$.

Each block and noise components are explained next in detail.

2.1 Neuro-spike Communication: Axonal Transmission

An experiment on the axonal transmission for CA region of the hippocampal [21] helps us understand the axonal behavior of thin, unmyelinated hippocampal place cells. The results of the experiment are as follows. For a low frequency firing rate, spikes propagate through the axon without any amplitude distortion, and nearly no failure occurs. On the other hand, for high frequency firing rate, if the inter-spike interval diminishes, the amplitude of the higher order spikes decreases logarithmically.

Moreover, the experiment shows that the time delay in the higher order spikes are much greater with respect to the initial spikes. In another study, it is stated that consecutive spikes lower the conduction velocity leading to the latency for higher order spikes [19]. Thus, if the spike frequency increases, the time delay rises as well. As a result, the spikes are distorted in both amplitude and time or undistorted depending on the spike frequency when propagating along the axon.

It is deduced from the results of the experiment that the axon can be modeled as a low pass filter, because the amplitude of the higher order spikes are attenuated and finally disappear associated with the increasing spike frequency.

In order to describe a low pass filter, we have to specify the magnitude and phase response characteristics. The magnitude response is extracted from the experiment in [21], assuming that the attenuation occurs due to consecutive spikes, implying that the effect of spikes which are far away from each other can be neglected. For the phase response, we know that the smaller the inter-spike interval the lower the time delay. Although the time delay is not known exactly for each spike in a spike train, we know that delay increases with frequency.

Hence, the axon acts as a modified version of a second order Butterworth low pass filter. The main reason of choosing this filter is that, the second order Butterworth filter amplitude response is constant at some point, and then, begins to decline with a rate similar to the above experimental data. This means, lower spike frequency produces no distortion up to some value whereas higher frequency distorts the amplitude which reflects the behavior of the axon. The other reason of choosing this filter is due to the time delay characteristics. The second order Butterworth low pass filter's

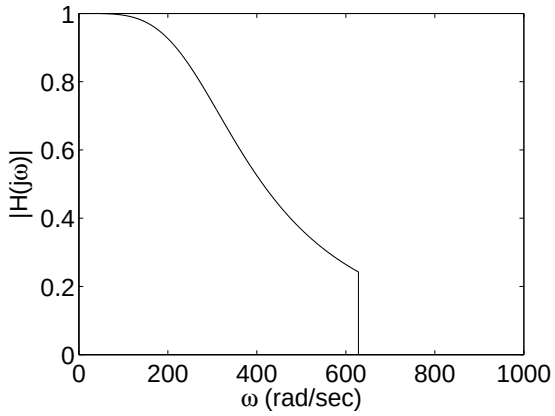

Figure 2.3: Magnitude response of the modified second order butterworth low pass filter.

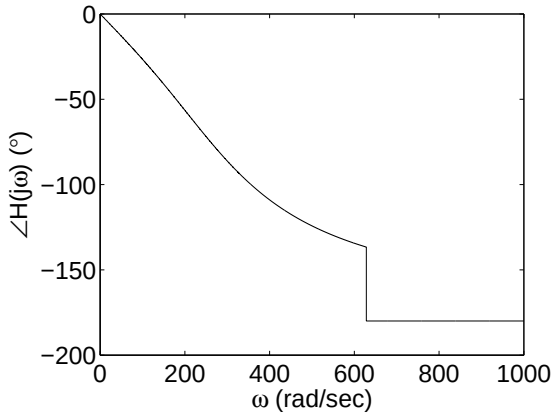

Figure 2.4: Phase response of the modified second order butterworth low pass filter.

phase response shows linear increase with frequency. Thus, it is compatible with the time delay characteristics in the axon. It is modified because after some point the magnitude response jumps to zero which is the consequence of the refractory period.

A normalized sample transfer function of the modified second order Butterworth filter that characterizes the axonal transmission, shown in Figure 2.3 and 2.4, is given as

$$H(jw) = \frac{a}{-w^2 + jbw + a}[u(jw) - u(jw - c)] \tag{2.1}$$

where $u(.)$ is the unit step function and the a, b, c are arbitrary values taken as $a = 314.15^2$, $b = 444.28$, and $c = 628.3$, similar to the experiment in [21].

There is a functional similarity between low pass anti-aliasing filter and axonal filter

that achieves the elimination of the spikes which have smaller inter-spike intervals. High usage of the channel within short time results in the depletion of the synaptic sources and the vesicle release probability decreases. After some point, a vesicle is not secreted in response to a spike. Spikes that do not cause the vesicle release are not distinguished at the output and this leads to the aliasing.

The low pass filter proposed for the axonal transmission decreases the depletion level of the synaptic sources and the vesicle release probability increases depending on the decrease in the frequency of an incoming stimuli train.

Filtering the higher frequency components to reduce the undistinguished inputs is well suited to the behavior of an anti-aliasing filter.

In the physical channel model, axonal transmission is implemented as follows. Firstly, the impulse train is converted to rectangular pulses such that when an impulse comes, the pulse level goes high assuming the pulse is initially in low state. It remains there until the next impulse and goes to low state for the next incoming impulse. It repeats the same procedure for all impulses. Secondly, these rectangular pulses pass through the anti-aliasing filter, and lastly, pulses are converted to impulses again. The main rational behind the state transition between impulses and rectangular pulses is to filter the impulses having lower inter-spike interval by the anti-aliasing filter. This part is shown in Figure 3.1(a).

2.2 Neuro-spike Communication: Synaptic Transmission

Synaptic transmission is composed of three parts, namely vesicle release, diffusion and EPSP generation.

2.2.1 Vesicle Release

Neurotransmitters are released from presynaptic terminal to the synapse as packets. These neurotransmitter packets are called *vesicles* or *quanta*. There are two important definitions related with the quanta, the first one is the quantal content that is the average number of quanta generated in response to a spike. The second one is the

quantal size or quantal amplitude that is the synaptic response to a single quantum.

It is important to determine the quantal analysis, i.e., quantal content and quantal size as well as the release probability of the quanta from the presynaptic terminal in order to model the release structure of the neurons at the CA region of the hippocampus. Therefore, the quantal analysis and the release probability are discussed next.

2.2.1.1 Quantal Analysis

Vesicles are secreted in special areas of the presynaptic terminal called active zones. The release occurs at this zone and the number of total active zones per presynaptic terminal determine the quantal content in response to a spike. The majority of neurons located at the hippocampus have one single active zone per presynaptic terminal [24]. Furthermore, hippocampal pyramidal neurons release one or zero quantum from a single active zone in response to an incoming spike [26]. Hence, a spike propagating along the axon and arriving the presynaptic terminal causes to release either one or zero quantum from the active zone depending on the vesicle release probability.

The quantal size specification is more intricate than the quantal content in the hippocampal CA neurons. In standard Katz model, it is stated that the quantal size in the neuromuscular junction of the frog is constant [11]. However, this is not valid for hippocampal CA neurons. The quantal size is not constant and varies from one quanta to the other. This leads to the amplitude fluctuations at the output neuron, which is discussed in Section 2.2.3.

2.2.1.2 Vesicle Release Probability

Vesicle release has a random nature. Even if a spike comes to a presynaptic terminal, a vesicle may not be generated. Conversely, if a spike does not come, a vesicle may be generated spontaneously. However, the probability of spontaneously occurred vesicle is very low for hippocampal neurons [17], therefore, it can be ignored.

Synaptic plasticity leads to the change in the behavior of the synapse. Short term plasticity and long term plasticity are two main types of synaptic plasticity.

The short term synaptic plasticity takes an important role for the vesicle release probability. The spike train coming continuously from the axonal branch affects the transmission by some special mechanism of the short term plasticity called *facilitation* and *depletion* [7]. If the initial release probability is lower and when stimuli trains come, firstly the response increases due to the facilitation, and then, decreases due to the depletion. On the other hand, if the initial release probability is higher, facilitation does not occur and when stimuli trains come, the response continuously decreases due to depletion. The release probability for hippocampal neurons [3] is low, thus it exhibits the former behavior. In the same study, it is shown that facilitation and depletion are presynaptic events, so the response to a single quantum does not change under the facilitation and depletion conditions.

The long term synaptic plasticity, associated with the learning and memory functions, classified as a postsynaptic event and mentioned in Section 2.2.3.

Vesicle release function of the neuro-spike communication is represented as packet generation in the physical channel model. It refers to the converting the continuous spikes to the packet sequence shown in Figure 3.1(b).

Packet release is a random process depending on inter-spike interval (γ) and channel utilization or state (S).

For each given γ value, the outcome has a different release probability, r_k, associated with the S. If the packet number in the synapse rises, i.e., the use of channel rises, the probability initially increases, and then, decreases. This characteristics of the probabilistic packet release function with respect to S for a given γ value can be formed similar to the study in [7] such that

- The initial vesicle release probability for incoming spike is p_0.

- The release probability exponentially increases after the first release depending on the facilitation.

- After facilitation, there is an exponential decrease associated with the depletion such that the decrease rate is smaller than the increase rate.

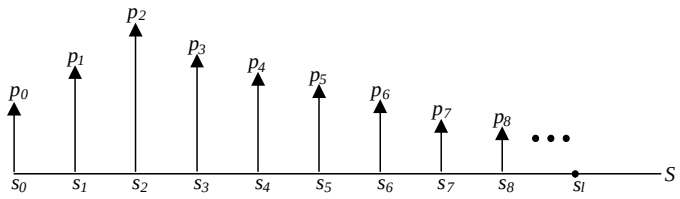

Figure 2.5: The probabilistic release function in terms of S for a given γ, assuming that at s_2 facilitation stops and depletion begins.

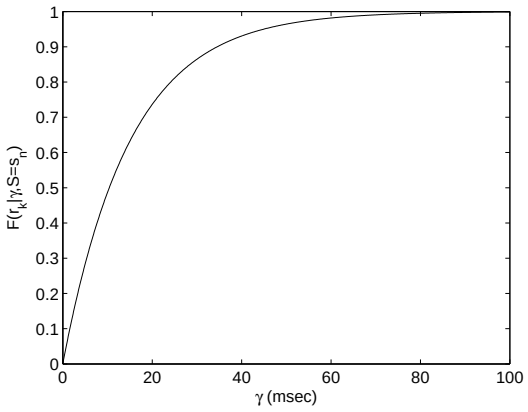

Figure 2.6: The probability distribution function of $F(r_k|\gamma, S = s_n)$.

This probabilistic packet release function with respect to S for a given γ is observed in Figure 2.5.

The p_0, p_1, p_2, $\cdots$ values may change for different γ, however, the general behavior of the probability function is same for all γ.

Similarly, for each given S, the outcome has a different release probability changing with γ value. In accordance with the results of the existing experiments [28], [29], the decrease in γ causes approximately exponential decline in the Excitatory PostSynaptic Current (EPSC), which is the excitation due to the charged ions in the terminal. This reduction is related with the lower release probability. We model this behavior depending on the γ for a given S as having an exponential probability distribution such that

$$F(r_k|\gamma, S = s_n) = (1 - exp(-\gamma|\mu))u(\gamma) \tag{2.2}$$

This is drawn in Figure 2.6 for $\mu = 15$.

2.2.2 Diffusion

Once vesicle is released, the glutamate type neurotransmitters included in the vesicle are diffused through the synapse. Let x_n be the n^{th} vesicle released from the presynaptic terminal containing j number of glutamate molecules such that

$$x_n = [x_{n1} x_{n2} \cdots x_{nj}] \tag{2.3}$$

From (2.3), x_n can be written as

$$x_n = \sum_{i=1}^{j} x_{ni} \delta(n - n_i) \tag{2.4}$$

where each x_{ni} refers to one neurotransmitter.

From (2.4), each neurotransmitter behaves like a point source. Assuming that the diffusion occurs in homogeneous medium at 1 dimension, the diffusion of each particle x_{ni} at point R_i at time t is solved by the Green's function that exhibits the Gaussian diffusion in response to particles, i.e.,

$$G(R_i^f - R_i, t) = \frac{1}{\sqrt{4\pi t}} exp(\frac{-(R_i^f - R_i)^2}{4t}) \tag{2.5}$$

where R_i^f is the destination position of the particle.

Hence, the diffusion of each glutamate particle is found as

$$x_{ni}(R_i^f, t) = \int_{-\infty}^{\infty} x_{ni}(R_i, t) G(R_i^f - R_i, t) dR_i \tag{2.6}$$

Whether a neurotransmitter can excite a potential on the output or not depends on the receptors, because they may be saturated or in a closed state. This issue is further investigated in Section 2.2.3.

The diffusion of neurotransmitters are taken as diffusive propagation in the physical channel model shown in Figure 3.1(c).

2.2.3 EPSP Generation

Diffused neurotransmitters affect the output neuron via the receptors on it. There are two main types of receptors on the output neuron. One is ionotropic receptors, the

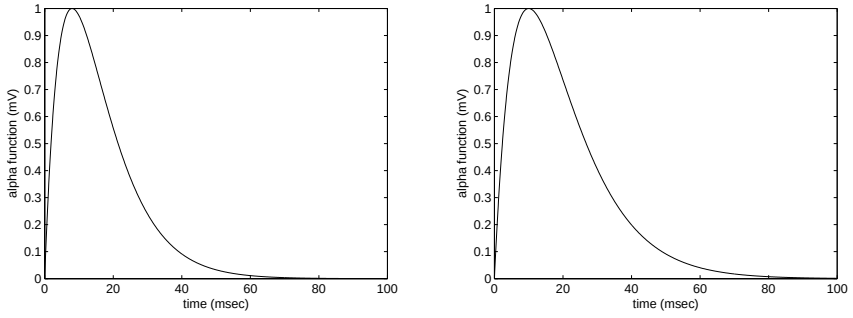

(a)

(b)

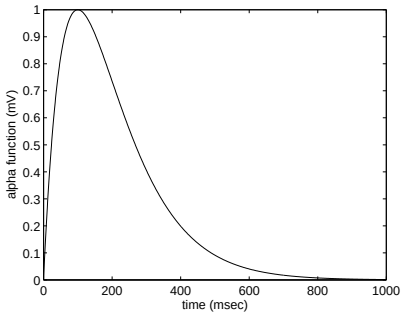

(c)

Figure 2.7: Receptors response, (a) The AMPA response, (b) The NMDA response, (c) The mGluR response.

other is metabotropic receptors.

For the ionotropic receptors, the neuron is excited by direct binding of neurotransmitter to the receptor. The examples of ionotropic receptors for the glutamate are Alpha-Amino-3-Hydroxy-5-Methyl-4-Isoxazole-propionate (AMPA), N-Methyl-D-Aspartate (NMDA) and kainate where the AMPA and NMDA are the basic ones.

Neurotransmitters bind to the receptors on postsynaptic terminal and lead to the opening of ion channels and flow of positively charged ions into the terminal. The flow of ions through the terminal causes EPSC. Furthermore, the flow of ions causes temporary membrane depolarization called EPSP.

The postsynaptic current provides conductance change at the output neuron, which is

an alpha function [5], [22] such as

$$g(t) \propto \frac{t}{\tau} exp(1 - \frac{t}{\tau}) u(t) \tag{2.7}$$

where τ is some constant associated with the type of the receptor.

The normalized analog voltage waveform in response to one neurotransmitter for the AMPA type receptor is

$$\alpha_A(t) = \frac{t}{\tau_1} exp(1 - \frac{t}{\tau_1}) u(t) \tag{2.8}$$

For NMDA type receptor, the change in conductance is slightly different than the AMPA type because its activation and deactivation are smaller. Moreover, its effect depends on the depolarization level of the output neuron.

The normalized analog voltage waveform in response to one neurotransmitter for the NMDA type receptor is

$$\alpha_N(t) = \frac{t}{\tau_2} exp(1 - \frac{t}{\tau_2}) u(t) \tag{2.9}$$

where $\tau_2 > \tau_1$.

The activation of the NMDA receptors depend on the long term plasticity or long term potentiation (LTP). Long term potentiation means the enhancement in the signal transmission in a long time. LTP occurs when two events occur simultaneously. The first one is the sufficient depolarization level at the terminal to reduce the Mg^{2+} from NMDA and the second one is the incoming glutamate that binds the NMDA channel [4].

In addition to the ionotropic receptors, there are metabotropic glutamate receptors (mGluRs) whose mechanism differs from the ionotropic ones. The effects of metabotropic receptors are very slow and they act indirectly through the special proteins or the second messenger system [11].

In case of metabotropic type receptors, the general waveform shape appears like an alpha function, however, the decay rate is much slower than the ionotropic ones [11].

The normalized analog voltage waveform in response to one neurotransmitter for the metabotropic receptor is

$$\alpha_{mGluR}(t) = \frac{t}{\tau_3} exp(1 - \frac{t}{\tau_3}) u(t) \tag{2.10}$$

where $\tau_3 \gg \tau_1, \tau_2$.

We draw the normalized alpha functions such that $\tau_3 \gg \tau_2 > \tau_1$ for $\tau_1 = 8$, $\tau_2 = 10$, $\tau_3 = 100$. The graphs are in Figure 2.7(a), 2.7(b), 2.7(c).

The $\alpha_{mGluR}(t)$ affects the output neuron in much longer time than the others. Furthermore, the metabotropic receptors are rare with respect to the AMPA and NMDA, and they are not observed at every postsynaptic terminal [11]. Actually, the AMPA and the NMDA are the main receptors that provide the excitation for glutamate type neurotransmitters [5]. Therefore, mGluRs can be neglected.

Each neurotransmitter is mapped to continuous analog signal during the transmission of spikes. This behavior resembles the modulator in digital communication. Therefore, the generation of EPSP waveform from neurotransmitters will be modeled as modulator in the physical channel model illustrated in Figure 3.1(d).

The response to several vesicles are not taken as simply the linear sum of the individual vesicle responses because this response can vary from vesicle to vesicle which is called the trial-to-trial variability.

Quantal size of each vesicle, the state of the receptors, i.e., opening probability of receptors, the number of available receptors at the postsynaptic terminal, the receptors desensitization, whether or not the diffused neurotransmitters bind to the receptors have an effect on the magnitude of the response. Since they have random nature, the response to a single vesicle, which creates the EPSP, varies from trial-to-trial [2].

In the physical channel model, trial-to-trial variability of the amplitude is implemented as random amplitude distortion block illustrated in Figure 3.1(e).

2.3 Neuro-spike Communication: Noise Components and Spike Generation

The noise components and spike generation are explained in this part.

2.3.1 Noise Components

There are two major sources of noise in neuro-spike communication. One is due to the axon, i.e., axonal noise and the other is due to the synapse, i.e., synaptic noise.

2.3.1.1 Axonal Noise

Pyramidal cell axons have very small diameter around $0.3\mu m$ and they are more prone to noise for this reason [9]. Therefore, noise heavily affects the axonal transmission, and it has to be taken into account in neuro-spike communication.

Channel noise, stemming from the stochastic opening and closing of voltage gated ion channels [6], is the most dominant noise source [17]. In case of the channel noise, spontaneous action potential occurs depending on the randomly opening of the sufficient number of Na^+ channels which is independent of the type of the axon model [9].

Furthermore, thermal noise due to the thermal agitations of electrons in a circuit, shot noise incurred by random fluctuations in dc current, and other membrane noises [17] also contribute to the total noise in the axon. However, they are not taken into account because their effects are negligible compared to the channel noise.

2.3.1.2 Synaptic Noise

The noise in the synapse and the dendrite, where the postsynaptic terminal is located, constitutes the synaptic noise. The basic source of the synaptic noise is the background synaptic activity which is due to the extreme synaptic effect from thousands of other synapses [10], [17]. On the other hand, the fundamental type of noises in the dendrite are the channel noise due to stochastic opening and closing of ligand-gated ion channels, thermal noise and shot noise. Similar to the axonal noise, there are also some other membrane noises as well. From these noise sources, background synaptic noise most heavily affects the output signal with respect to the other noise sources [17].

Synaptic background noise covers the effect of many different synapses. Therefore, its probability density function converges to the Gaussian due to the central limit theorem. Hence, synaptic noise is modeled as Gaussian process.

2.3.2 Spike Generation

In order to fire a spike at the output, it has to be sufficiently depolarized. However, the generated EPSP due to only one active receptor is not sufficient to form a spike. Therefore, a spike is formed by the temporal summation or spatial summation of the group of active receptors' responses in the same postsynaptic terminal.

Temporal summation means the effect of neurotransmitters released from the same presynaptic terminal to the same postsynaptic terminal with different arrival times. On the other hand, spatial summation refers to the effect of different presynaptic terminals on the same postsynaptic terminal.

In the physical channel model, spatial summation does not have any effect because the channel is modeled between only one presynaptic and postsynaptic terminal.

The spike generation block of neuro-spike communication is represented as the receiver that provides the spikes from the incoming excitations shown in Figure 3.1(f).

CHAPTER 3

PHYSICAL CHANNEL MODEL OF NANOSCALE NEURO-SPIKE COMMUNICATION

An input neuron has many presynaptic terminals meaning that it leads to the excitation in many postsynaptic terminals. However, we consider the channel among the input neuron axon, one single presynaptic terminal of the input neuron and one single postsynaptic terminal of the output neuron. Therefore, it can be classified as a single input single output (SISO) channel. It involves all the steps from the transmission of impulses along the input neuron axon until the generation of impulses at the output neuron.

This SISO channel is modeled in terms of the communication theory subsystems in Figure 3.1, where each block represents major functionalities of the neuro-spike communication at the CA region.

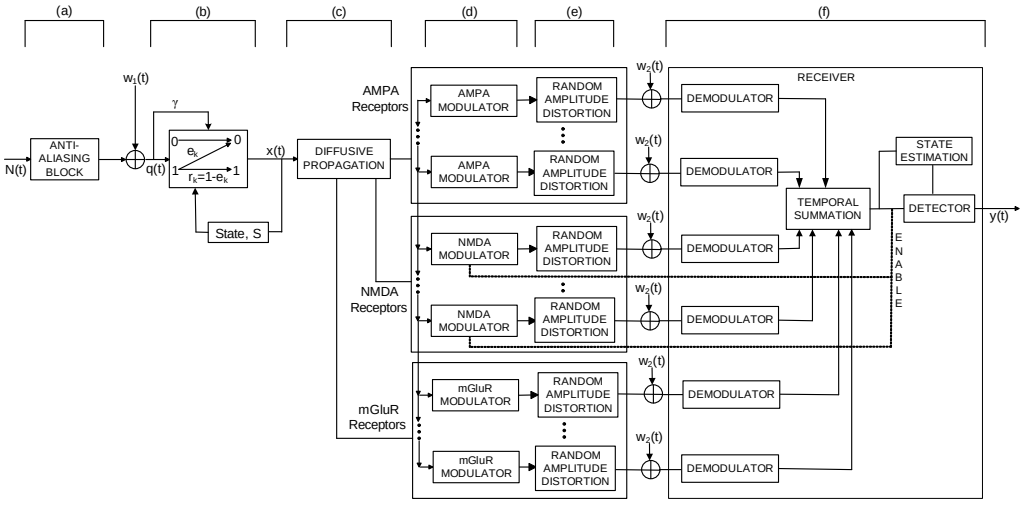

Figure 3.1: The physical channel model.

In this channel model, channel source is encoded as impulses. These impulses are passed through the anti-aliasing block, which consists of state transition from impulses to rectangular pulses, anti-aliasing filter and state transition from rectangular pulses to impulses. After that, impulsive axonal noise is added and the resultant impulse train reaches the presynaptic terminal.

At the presynaptic terminal, packets are either released or not in response to these incoming impulses to the terminal. The probability of packet release depends on γ and state, S. The incoming impulse and release of the packet are denoted as 1 in Figure 3.1(b).

The released packet includes many neurotransmitters, each of which is subject to diffusion and binds one of the receptors.

According to the affected receptors, the response shows difference. Moreover, for NMDA receptors, an enable signal is needed to activate them. They are passive, i.e., closed without this enable signal.

A continuous signal is generated by each neurotransmitter in response to receptors. Due to trial-to-trial variability, the signal incurs random amplitude distortion and the synaptic noise is added to it before reaching the receiver.

All of the signals obtained from different receptors for one packet are summed and EPSP is generated at the postsynaptic terminal. In response to this EPSP, an impulse is generated at the receiver.

3.1 Analysis of the Physical Channel Model

In this part, we specify the input-output relation of the channel by deriving the input impulse train detection probability at the output and channel delay. After that, an information theoretical analysis is performed for the packet release mechanism of the channel.

3.1.1 Input-Output Relation of the Channel

Any excitation above the threshold level of the input neuron at the CA region of the hippocampus generates impulses at the neuron axon. The arrival of this excitation to the input neuron is a stochastic process. Since there may be numerous independent sources that produce the excitation, this stochastic model can be taken as Poisson process. Furthermore, the arrival of the stimuli can result no impulse, one impulse or more than one impulse independent of time, this is to say the firing rate of the neuron is itself a stochastic process as well. This does not resemble the classical Poisson process with deterministic intensity fuction. In this case, the intensity is a random stationary function. This process is called as doubly stochastic Poisson process, which is a point process.

A point process, which is the derivative of a counting process, is represented as the sum of impulses. Each impulse corresponds to the occurrence of one event at time t.

Similar to the input of the neuron, the modeled channel input is taken as impulse trains consistent with the doubly stochastic Poisson process. Eventually, the input of the channel is a random process $N(t)$ where $\{N(t), [0, T]\}$ is a point process, particularly doubly stochastic Poisson process with a non-negative random stationary intensity function, λ_n.

The channel input is given by

$$N(t) = \sum_{k} \delta(t - t_k) \tag{3.1}$$

$\{t_0, t_1, t_2, t_3, ...\}$ is a random sequence.

The probability of event occurrence at time t_k and the correlation among t_k and t_j rely on the λ_n random intensity function of the doubly stochastic Poisson process.

The mean, $E[N(t)]$, and autocorrelation function, $R_{N(t)}$, of $N(t)$ is derived in Appendix A and can be written as

$$E[N(t)] = E[\eta] \tag{3.2}$$

$$R_{N(t)} = E[\eta_1 \eta_2] \tag{3.3}$$

where η, η_1 and η_2 are the integrals of λ_n from time t, t_1, t_2 to t_x, respectively.

The probability of an impulse train having i impulses at $N(t)$ in $[0, T]$ is

$$P(N(t) = i) = \frac{exp(-E[\eta])(E[\eta])^i}{i!} \tag{3.4}$$

The anti-aliasing filter has an impulse response $h(t)$ defined in accordance with (2.1) and its output is $N_a(t)$. The mean, $E[N_a(t)]$, and autocorrelation function, $R_{N_a(t)}$, of the output are expressed as

$$E[N_a(t)] = E[N(t)] * h(t) \tag{3.5}$$

$$R_{N_a(t)} = R_{N(t)} * h(t) * h(-t) \tag{3.6}$$

The signal in the presynaptic terminal of the input neuron, $q(t)$ is

$$q(t) = N_a(t) + w_1(t) \tag{3.7}$$

where $w_1(t)$ is the axonal noise such that $w_1(t) = \delta(t - t_m)$.

The channel is analyzed in a limited interval, $[0, T]$, therefore, we assume that at most one spike occurs in this interval due to the axonal noise.

Since axonal noise mainly results from the stochastic opening of the ion channels, it is independent of the impulse propagation along the axon. Therefore, $N_a(t)$ and $w_1(t)$ are independent processes.

$q(t)$ can also be expressed as the sum of impulses like

$$q(t) = \sum_i q_i(t) \tag{3.8}$$

where $q_n(t) \propto \delta(t - t_n)$ which is taken as the n^{th} impulse, q_n in the packet generation mechanism.

The probability of an impulse train having i impulses at $q(t)$ in $[0, T]$ is

$$P(q(t) = i) = P(N(t) = i - 1)P_a + P(N(t) = i)(1 - P_a) \tag{3.9}$$

where P_a is the probability of an impulse occurrence due to axonal noise.

The mean and autocorrelation function of $q(t)$ are

$$E[q(t)] = E[N_a(t)] + E[w_1(t)] \tag{3.10}$$

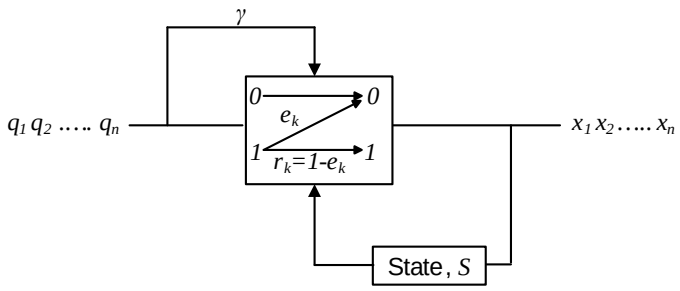

Figure 3.2: Packet generation mechanism.

$$R_{q(t)} = R_{N_a(t)} + R_{w_1(t)} + 2E[N_a(t)]E[w_1(t)] \tag{3.11}$$

Substituting (3.5), (3.6) in (3.10) and (3.11) yield

$$E[q(t)] = E[N(t)] * h(t) + E[w_1(t)] \tag{3.12}$$

$$R_{q(t)} = R_{N(t)} * h(t) * h(-t) + R_{w_1(t)} + 2(E[N(t)] * h(t))E[w_1(t)] \tag{3.13}$$

The analysis up to now reveals the relation between $N(t)$ and $q(t)$. Now, we observe the effect of any impulse $q(t)$, at the output, $y(t)$ by dividing the channel into 3 subportions, namely packet generation mechanism, synapse and receiver.

3.1.1.1 Packet Generation Mechanism

The packet generation mechanism of the channel in response to an impulse is shown in Figure 3.2. Each input q_m and each output x_m have a binary alphabet such that 1 denotes the incoming impulse for the input and released packet for the output, whereas 0 symbolizes no impulse for the input and no released packet at the output. The vesicle release probability, r_k between each impulse q_m and each packet x_m mainly depends on γ and S. γ can be extracted from the input and state information, S, is taken from the output as a feedback.

According to the usage of channel, there exist finite, i.e., $l+1$ different channel states, S such as

$$S = \{s_0, s_1, s_2, ..., s_l\} \tag{3.14}$$

where s_0 corresponds to an initial state and s_l refers to the state that no release occurs, i.e., $r_k = 0$.

The state transitions are stationary and depends only on previous state. Thus, $\{s_n, n = 0, 1, 2, ...\}$ is a stationary Markov process.

The packet generation structure is the combination of $l + 1$ channels having different states and release probabilities with the same input and output alphabet for a given γ. This binary input binary output alphabet finite state channel with Markov transitions is called Finite State Markov Channel (FSMC).

To describe a FSMC, $[l + 1\ X\ l + 1]$ transition matrix $\mathbf{T}$, $[1\ X\ l + 1]$ steady state probability matrix $\mathbf{P}$ and $[1\ X\ l+1]$ error matrix $\mathbf{e}$ have to be specified [27]. Transition matrix, $\mathbf{T}$ is given by

$$\mathbf{T} = \begin{bmatrix} P_{00} & P_{01} & 0 & 0 & . & . & . & 0 \\ P_{10} & P_{11} & P_{12} & 0 & . & . & . & 0 \\ P_{20} & 0 & P_{22} & P_{23} & . & . & . & 0 \\ . & . & . & . & . & . & . & . \\ . & . & . & . & . & . & . & . \\ P_{l0} & 0 & 0 & 0 & . & . & . & P_{ll} \end{bmatrix}$$

where P_{ij} is equal to the successful packet release when the channel is in state s_i for a specific γ such that

$$P_{ij} = P(x_m = 1|S = s_i, \gamma),\ j \neq i\ \&\ j \neq 0 \tag{3.15}$$

If a packet is not released, i.e., $x_m = 0$, the state does not change such that

$$P_{ii} = P(x_m = 0|S = s_i, \gamma) \tag{3.16}$$

Moreover, if it passes sufficient time and no release occurs, the state turns to the initial state. This probability is equal to $P_{i0}, \forall i$.

The sum of all these probabilities are

$$\sum_j P_{ij} = 1 \tag{3.17}$$

The steady state probability matrix, $\mathbf{P}$ is

$$\mathbf{P} = \begin{bmatrix} p_0 & p_1 & . & . & . & p_l \end{bmatrix}$$

where $P(S = s_i) = p_i$ and

$$\sum_i P(S = s_i) = 1 \tag{3.18}$$

The error probability, e_k, for each impulse is determined in accordance with γ and S. The conditional probability with respect to S for a given γ, $P(r_k|S, \gamma = \Gamma)$, or equivalently $P(x_m = 1|q_m = 1, S, \gamma = \Gamma)$ is drawn in Figure 2.5. The conditional probability distribution function with respect to γ for a given S, $F(r_k|\gamma, S = s_n)$ or $F(x_m = 1|q_m = 1, \gamma, S = s_n)$ is given in Figure 2.6. In compatible with these, error matrix, i.e., **e** is represented as

$$\mathbf{e} = \begin{bmatrix} e_1 & e_2 & . & . & . & . & e_l \end{bmatrix}$$

where

$$e_k = \int_0^\infty \sum_m P(x_m = 0|q_m = 1, s_k, \gamma) P(S = s_k) f_\gamma(\gamma) d\gamma \tag{3.19}$$

where $f_\gamma(\gamma)$ is the probability density function of the γ.

Hence, the release probability is

$$r_k = 1 - e_k \tag{3.20}$$

3.1.1.2 Synapse

After the release of the packet to the synapse, the issue is the excitation of a potential at the output by this packet. This behavior is illustrated in Figure 3.3.

Any released packet, x can be considered as a [1 X j] matrix written as (2.3). It can be divided into j neurotransmitters, i.e., j independent [1 X 1] matrix, x_i.

x_i can be treated as a point source at position R_i such that

$$x_i = \delta(R - R_i) \tag{3.21}$$

x_i diffuse through the synapse to the target neuron. The neurotransmitter that arrive to the target neuron x_i^d is written as

$$\begin{aligned} x_i^d &= \int \delta(R - R_i) G(R_i^f - R_i, t) dR_i \\ &= G(R_i^f - R_i, t) = \frac{1}{\sqrt{4\pi t}} exp(\frac{-(R_i^f - R_i)^2}{4t}) \end{aligned} \tag{3.22}$$

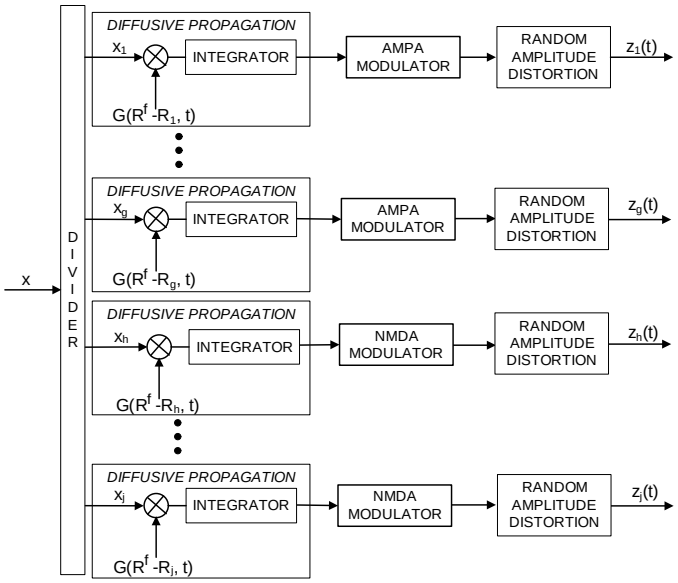

Figure 3.3: Synapse.

If a packet releases successfully from the presynaptic terminal, the probability of the incoming neurotransmitter at time θ_i to the output neuron for a determined R_i^f and R_i is

$$P(t = \theta_i) \propto \frac{1}{\sqrt{4\pi\theta_i}} exp(\frac{-b^2}{4\theta_i}) \tag{3.23}$$

where b is some constant equal to $(R_i^f - R_i)$.

θ_i corresponds to the random diffusion time and its probability density function is

$$f_{\theta_i}(\theta_i) = \frac{a(b)}{\sqrt{4\pi\theta_i}} exp(\frac{-b^2}{4\theta_i}) \tag{3.24}$$

Neurotransmitters present in one packet affect many receptors. In the analysis, the effect of the mGluR receptors are ignored and we assume that

- The neurotransmitters from x_1 to x_g affect the AMPA receptors.
- The neurotransmitters from x_h to x_j affect the NMDA receptors.

The neurotransmitters that affect the AMPA receptors are modulated by AMPA modulator. Its signal waveform is given in (2.8) and drawn in Figure 2.7(a). This generated signal in response to one neurotransmitter is subject to the random amplitude

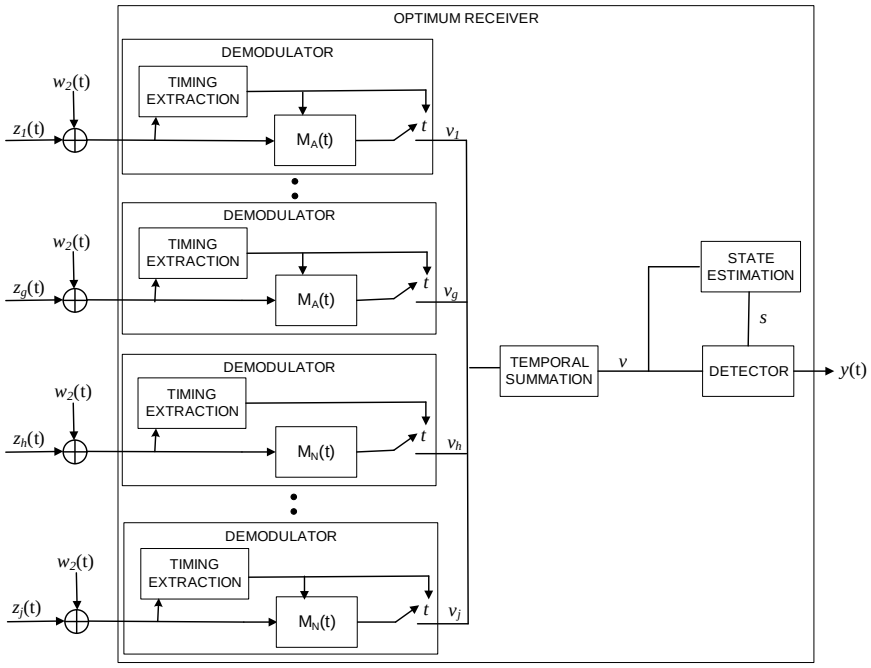

Figure 3.4: Optimum receiver.

distortion. Hence,

$$z_i(t) = d_i \alpha_A(t - \theta_i) \tag{3.25}$$

where d_i is due to the random amplitude distortion stemming from trial-to-trial variability of neurons for $1 \leq i \leq g$.

The modulation of the neurotransmitters in NMDA receptors are different than the AMPA. NMDA modulator's waveform is given (2.9) and drawn in Figure 2.7(b). Unlike the AMPA receptors, some activation time is required for the NMDA receptors. Thus, the waveform is shifted $t_0 > 0$. Therefore,

$$z_i(t) = d_i \alpha_N(t - t_0 - \theta_i), h \leq i \leq j \tag{3.26}$$

3.1.1.3 Receiver

Receiving structure of neuron is not known exactly, therefore, we design the optimum receiver for this channel model. The block diagram of the optimum receiver is given in Figure 3.4. The input of the receiver for any released packet in time between T_n

and T_{n+1} is

$$v_i(t) = z_i(t) + w_2(t), 1 \leq i \leq j \tag{3.27}$$

where $w_2(t)$ is white Gaussian noise.

$z_i(t)$ has random time delay, θ_i, therefore, it must be extracted before filtering.

Matched filter maximizes the signal-to-noise ratio (SNR) for additive white Gaussian noise (AWGN) case. Two types of matched filters are used for AMPA and NMDA modulators, namely $M_A(t)$ and $M_N(t)$ respectively. They are,

$$M_A(t) = \alpha_A(T_{n+1} - t + \theta_i), T_n \leq t \leq T_{n+1} \tag{3.28}$$

$$M_N(t) = \alpha_N(T_{n+1} - t + t_0 + \theta_i), T_n \leq t \leq T_{n+1} \tag{3.29}$$

The output of the matched filters pertaining to AMPA modulator for $T_n \leq t \leq T_{n+1}$ and $1 \leq i \leq g$ are

$$\begin{aligned} v_i &= \int_{T_n}^{T_{n+1}} d_i \alpha_A(\tau - \theta_i)\alpha_A(T_{n+1} - t + \theta_i + \tau)d\tau \\ &\quad + \int_{T_n}^{T_{n+1}} w_2(\tau)\alpha_A(T_{n+1} - t + \theta_i + \tau)d\tau \end{aligned} \tag{3.30}$$

The output of the matched filters of NMDA modulator for $T_n \leq t \leq T_{n+1}$ and $h \leq i \leq j$ are

$$\begin{aligned} v_i &= \int_{T_n}^{T_{n+1}} d_i \alpha_N(\tau - t_0 - \theta_i)\alpha_N(T_{n+1} - t + t_0 + \theta_i + \tau)d\tau \\ &\quad + \int_{T_n}^{T_{n+1}} w_2(\tau)\alpha_N(T_{n+1} - t + t_0 + \theta_i + \tau)d\tau \end{aligned} \tag{3.31}$$

From (3.30) and (3.31),

$$v_i = c_i d_i + n_i, 1 \leq i \leq j \tag{3.32}$$

where c_i and n_i for $1 \leq i \leq g$ are

$$c_i = \int_{T_n}^{T_{n+1}} \alpha_A(\tau - \theta_i)\alpha_A(T_{n+1} - t + \theta_i + \tau)d\tau \tag{3.33}$$

$$n_i = \int_{T_n}^{T_{n+1}} w_2(\tau)\alpha_A(T_{n+1} - t + \theta_i + \tau)d\tau \tag{3.34}$$

and for $h \leq i \leq j$ are

$$c_i = \int_{T_n}^{T_{n+1}} \alpha_N(\tau - t_0 - \theta_i)\alpha_N(T_{n+1} - t + t_0 + \theta_i + \tau)d\tau \tag{3.35}$$

$$n_i = \int_{T_n}^{T_{n+1}} w_2(\tau)\alpha_N(T_{n+1} - t + t_0 + \theta_i + \tau)d\tau \tag{3.36}$$

Each d_i is independent identically distributed (iid). Likewise, each n_i is iid as well. Moreover, d_i and n_i are independent from each other.

After the temporal summation

$$v = \sum_{i=1}^{j} v_i \tag{3.37}$$

To make a decision, state estimation is also needed. We show that it can be calculated recursively at the output.

The current channel state, s_n is found recursively by using the previous output of the matched filters, v^{n-1}, and the previous states, s^{n-1}, such that

$$P(s_n|v^{n-1}, s^{n-1}) = \frac{P(v_{n-1}, s_n|v^{n-2}, s^{n-1})P(v^{n-2}, s^{n-1})}{P(v^{n-1}, s^{n-1})} \tag{3.38}$$

It can be written as

$$P(s_n|v^{n-1}, s^{n-1}) = P(v_{n-1}|v^{n-2}, s_n, s^{n-1})\frac{P(s_n|v^{n-2}, s^{n-1})P(v^{n-2}, s^{n-1})}{P(v^{n-1}, s^{n-1})} \tag{3.39}$$

Since v does not depend on the next channel state, the first term of the numerator is converted to

$$P(v_{n-1}|v^{n-2}, s_n, s^{n-1}) = P(v_{n-1}|v^{n-2}, s^{n-1}) \tag{3.40}$$

The current channel state only depends on previous state and previous output of the matched filters, therefore, the second term of the numerator in (3.39) is simplified to

$$P(s_n|v^{n-2}, s^{n-1}) = P(s_n|s_{n-1}) \tag{3.41}$$

From the stationarity property of the state transitions, $P(s_n|s_{n-1}) = \mathbf{T}$, hence

$$P(s_n|v^{n-1}, s^{n-1}) = \frac{P(v_{n-1}|v^{n-2}, s^{n-1})\mathbf{T}P(v^{n-2}, s^{n-1})}{P(v^{n-1}, s^{n-1})} \tag{3.42}$$

The denominator of (3.42) be written as

$$P(v^{n-1}, s^{n-1}) = P(s^{n-1}|v^{n-1})P(v^{n-1}) \tag{3.43}$$

$P(s^{n-1}|v^{n-1})$ can be written as

$$P(s^{n-1}|v^{n-1}) = P(s_0)P(s_1|v_0, s_0)\cdots P(s_{n-1}|v^{n-2}, s^{n-2}) \tag{3.44}$$

Therefore,

$$P(s_n|v^{n-1}, s^{n-1}) = \frac{P(v_{n-1}|v^{n-2}, s^{n-1})\mathbf{T}P(v^{n-2}, s^{n-1})}{P(s_0)\prod_{i=1}^{n-2} P(s_i|v_{i-1}, s_{i-1})P(s_{n-1}|v^{n-2}, s^{n-2})P(v^{n-1})} \tag{3.45}$$

Hence, the current state is recursively calculated from the previous one.

Since the current state is probabilistically known, we prefer packet decision instead of sequence decision as a design criterion.

There are two hypotheses for each packet decision such that

$$H_1 : v = \sum_i c_i d_i + n_i, 1 \leq i \leq j \tag{3.46}$$

$$H_0 : v = \sum_i n_i, 1 \leq i \leq j \tag{3.47}$$

The threshold value, Ω for the decision rule is found by Neyman-Pearson method such that

$$\Omega = \frac{P(v|H_1)}{P(v|H_0)} \tag{3.48}$$

Since $(v|H_1)$ is the sum of many random variables, it is Gaussian due to the central limit theorem. Its mean and variance are

$$E[v|H_1] = \sum_i c_i E[d_i] = \mu \tag{3.49}$$

$$Var[v|H_1] = \sum_i c_i^2 Var[d_i] + Var[n_i] = \sigma_1^2 \tag{3.50}$$

Similarly, $(v|H_0)$ is Gaussian as well with the following mean and variance

$$E[v|H_0] = 0 \tag{3.51}$$

$$Var[v|H_0] = \sum_i Var[n_i] = \sigma_0^2 \tag{3.52}$$

Hence, the decision threshold, Ω, is

$$\Omega = \frac{\frac{1}{\sqrt{2\pi\sigma_1^2}} exp(-\frac{(v-\mu)^2}{2\sigma_1^2})}{\frac{1}{\sqrt{2\pi\sigma_0^2}} exp(-\frac{v^2}{2\sigma_0^2})} \tag{3.53}$$

which is further simplified to

$$\Omega = \frac{\sigma_0}{\sigma_1} exp(-\frac{(v-\mu)^2}{2\sigma_1^2} + \frac{v^2}{2\sigma_0^2}) \tag{3.54}$$

Taking logarithm of both sides,

$$\ln \Omega - \ln \frac{\sigma_0}{\sigma_1} + \frac{\mu^2}{2\sigma_1^2} = v^2(\frac{1}{2\sigma_0^2} - \frac{1}{2\sigma_1^2}) + v(\frac{\mu}{\sigma_1^2}) \tag{3.55}$$

Assign LHS and RHS to, *th* and *y*, respectively, i.e.,

$$\ln \Omega - \ln \frac{\sigma_0}{\sigma_1} + \frac{\mu^2}{2\sigma_1^2} = th \tag{3.56}$$

$$v^2(\frac{1}{2\sigma_0^2} - \frac{1}{2\sigma_1^2}) + v(\frac{\mu}{\sigma_1^2}) = y \tag{3.57}$$

where *th* is the threshold value and *y* is the sufficient statistics.

The optimum decision is based on the minimum probability of error, P_b, depending on current channel state and expressed by

$$P_b = P(y = 0|q = 1)P(q = 1) + P(y = 1|q = 0)P(q = 0) \tag{3.58}$$

P_b can also be written in terms of x, i.e.,

$$P_b = P(y = 0|x)P(x|q = 1)P(q = 1) + P(y = 1|x)P(x|q = 0)P(q = 0) \tag{3.59}$$

which can be rewritten as

$$P_b = [P(y = 0|x = 0)e_k + P(y = 0|x = 1)r_k]P(q = 1) + P(y = 1|x = 0)P(q = 0) \tag{3.60}$$

where

$$P(y = 0|x = 0) = P(y < th|x = 0) \tag{3.61}$$

$$P(y = 0|x = 1) = P(y < th|x = 1) \tag{3.62}$$

$$P(y = 1|x = 0) = P(y > th|x = 0) \tag{3.63}$$

Therefore, the probability of error, P_b, is

$$P_b = [P(y < th|x = 0)e_k + P(y < th|x = 1)r_k]P(q = 1) + P(y > th|x = 0)P(q = 0) \tag{3.64}$$

The output, $y(t)$ is a point process as well as $N(t)$. The probability of impulse train at $y(t)$ due to $q(t)$ having i impulses, found in (3.9), is

$$P(y(t) = i) = (1 - P_b)^i \tag{3.65}$$

Thus, the probabilistic analysis of detecting input impulse train is obtained with (3.4), (3.9), (3.65).

Moreover, the average impulse transmission rate, I_r, can be expressed by

$$I_r = \sum_i P(N(t) = i)(1 - P_b)^i \tag{3.66}$$

The channel delay brings some latency for the transmission of each impulse. It is equal to the sum of the delay while propagating through the axon of the input neuron and random diffusion time, θ_i, at synapse. The delay due to axon can be found using the filter in Figure 2.4, and random diffusion time is calculated via its probability density function found in (3.24). Eventually, each impulse at $y(t)$ incurs latency with respect to $N(t)$.

3.1.2 Information Theoretical Analysis for the Packet Released Mechanism

Different pattern of input impulse train, stemming from λ_n, leads to the uncertainty in P_b. To reduce this uncertainty, arising from the different inputs, the mutual information of packet released mechanism have to be increased.

To increase the mutual information between the impulse train, $q_1 q_2 \cdots q_n$, and packet sequence, $x_1 x_2 \cdots x_n$, mutual information is found conditionally in terms of an auxiliary parameter, ρ_n, defined as

$$\rho_n = P(s_n | x^{n-1}, s^{n-1}) \tag{3.67}$$

ρ_n resembles the parameter that is used in state estimation. The only difference is the output of the matched filters, v, is replaced with released packet, x. Hence, ρ_n is calculated recursively as well and known by the channel. Therefore, mutual information is expressed conditionally on ρ_n.

It is found in Appendix B that

$$I(q^n; x^n | \gamma) = \sum_{i=1}^{n} [H(x^i | \rho_i, \gamma) - H(x^i | q^i, \rho_i, \gamma)] \tag{3.68}$$

Note that (3.68) is obtained for a given γ. The mutual information between the spike trains in the presynaptic terminal and correspondent packet sequence is

$$I(q^n; x^n) = \int_0^\infty I(q^n; x^n | \gamma) f_\gamma(\gamma) d_\gamma \tag{3.69}$$

It is concluded in (3.69) that the mutual information can be derived as conditioned on the parameter which is calculated recursively by the channel. This leads to an increase in mutual information. Higher mutual information between the impulses at presynaptic terminal and the released packets at synapses reduce the uncertainty at r_k. Therefore, P_b is expressed more accurately and channel becomes more independent from the input signal.

CHAPTER 4

NUMERICAL ANALYSIS OF THE CHANNEL MODEL

The main performance measure of the channel is P_b. The lower P_b, the more efficient channel we get. Hence, we observe the error probability of detecting an input impulse at the output. In addition to that, channel delay is investigated.

4.1 Probabilistic Analysis of Impulse Detection

Our aim is to show the effect of the probability of incoming impulse to the presynaptic terminal, $P(q = 1)$, the total number of affected AMPA, g, and NMDA receptors, $(j - g)$, the total synaptic noise, V_T, threshold value of the output neuron, ω, alpha function constants, τ_1, τ_2, and expected value of random variable d_i to P_b.

The variance of d_i is not observed, because it does not have any significant effect on the channel performance.

Unless otherwise stated, the channel parameters are fixed to some arbitrarily chosen values as shown in Table 4.1 where V_T is

$$\sum_i Var[n_i] = V_T \tag{4.1}$$

To prevent any interference between consecutive symbols T_{n+1} is taken as 100 regarding τ_1 and τ_2.

Since $(\frac{1}{2\sigma_0^2} - \frac{1}{2\sigma_1^2}) << \frac{\mu}{\sigma_1^2}$, the sufficient statistics in (3.57) is reduced to

$$y = v(\frac{\mu}{\sigma_1^2}) \tag{4.2}$$

Table 4.1: Fixed arbitrarily chosen values for channel parameters

τ_1	8
τ_2	10
T_{n+1}	100
T_n	0
Total number of affected AMPA receptors (g)	25
Total number of affected receptors (j)	30
Mean value of d_i ($E[d_i]$)	0.5
Variance of d_i ($Var[d_i]$)	1/64
Total variance of synaptic noise (V_T)	0.3
$P(q = 1)$	0.8
$P(q = 0)$	0.2
ω	5

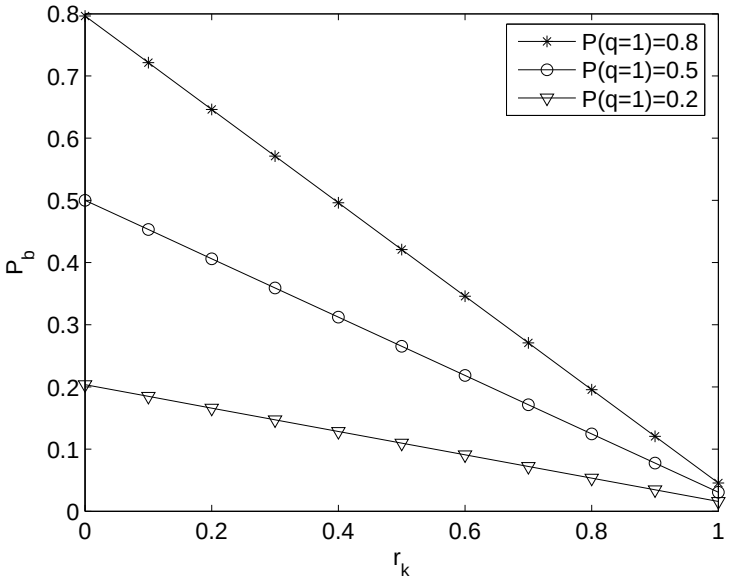

Figure 4.1: The effect of P(q=1) to the channel performance.

and calculations are performed accordingly.

In Figure 4.1, the effect of the probability of incoming impulse to the presynaptic terminal is illustrated. High impulse probability leads to increase in P_b. The result explains the importance of short term plasticity in a different point of view in terms of the P_b. Since short term plasticity prevents high ratio of packet release, it opposes the increase in P_b.

Figure 4.2 reveals the importance of the NMDA receptors. When the NMDA recep-

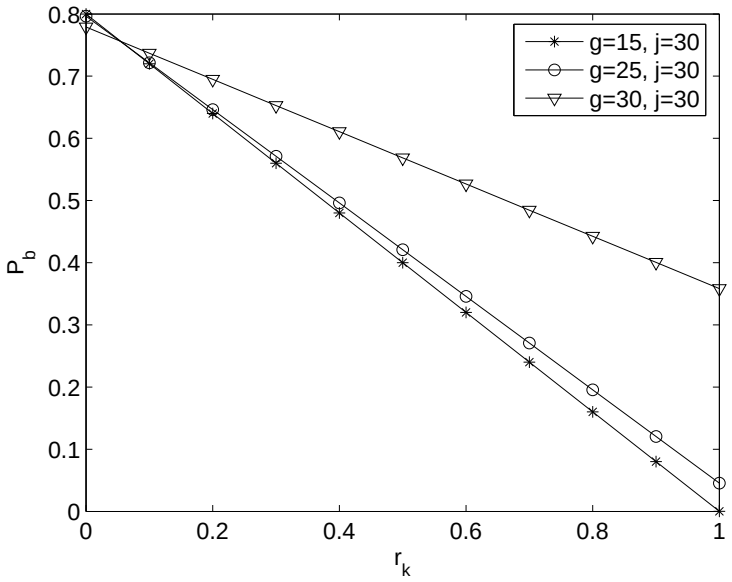

Figure 4.2: The effect of number of g and j to the channel performance.

tors are active, i.e., $(j - g) \neq 0$, the channel performance improves. This result is compatible with the long term plasticity in neurons. It means the enhancement in the signal transmission quality relying on the activation of the NMDA receptors.

The synaptic noise is observed in Figure 4.3. The increase in noise degrades the effect of neurotransmitters at the output receptors. Therefore, the input impulse may not be detected or an erroneous impulse is generated due to noise. Both of them lead to poor channel performance.

In Figure 4.4, the effect of ω on the channel performance is investigated. Although the increase in ω prevents to generate erroneous impulse due to noise, it complicates the detection of incoming neurotransmitters. Therefore, P_b slightly increases with increasing ω.

In Figure 4.5, greater values of τ_1, τ_2 constants result to higher excitation level at the receptors pertaining to output neuron. This facilitates the impulse detection at the output, and thus, channel performance improves.

The expected value of d_i has the response as in Figure 4.6. The increase in $E[d_i]$ means the reduction in amplitude distortion of EPSP. Therefore, P_b has a rapid de-

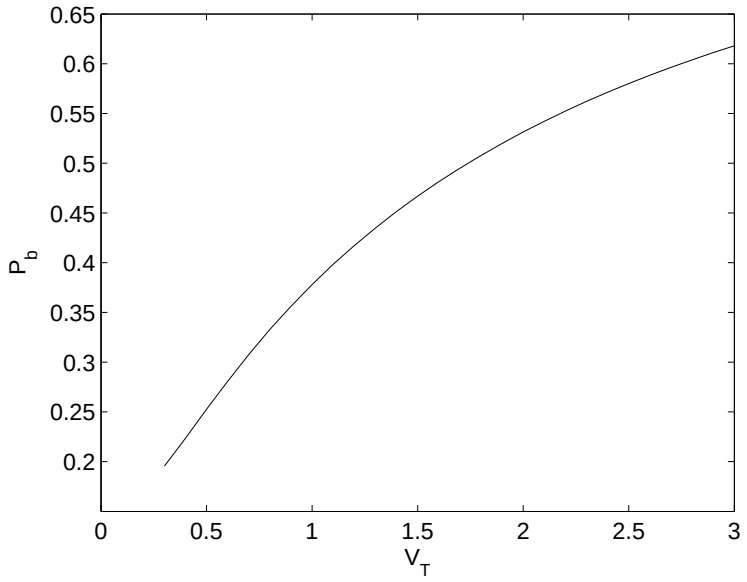

Figure 4.3: The effect of noise to the channel performance with $r_k = 0.8$.

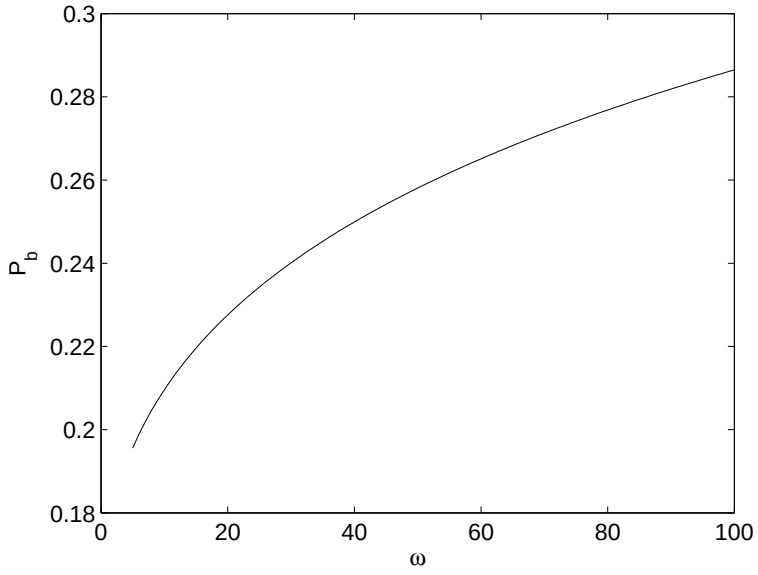

Figure 4.4: The effect of ω to the channel performance with $r_k = 0.8$.

cline, when $E[d_i]$ gets nearer to 1.

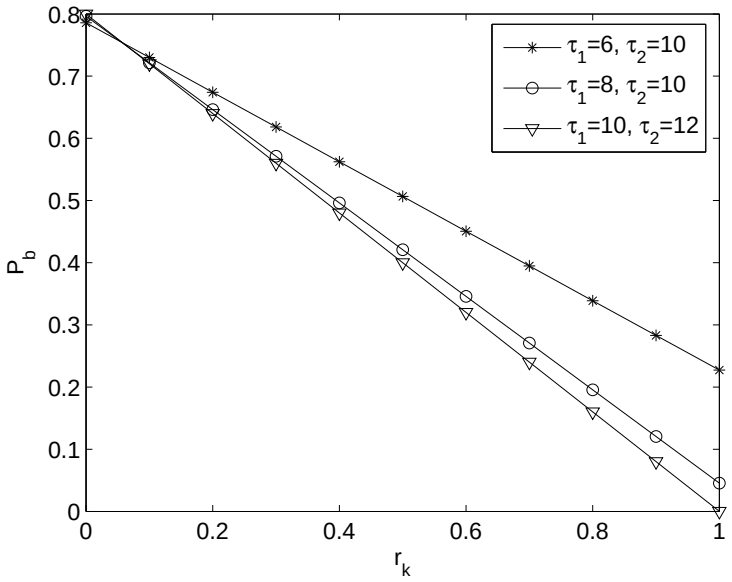

Figure 4.5: The effect of τ_1, τ_2 to the channel performance.

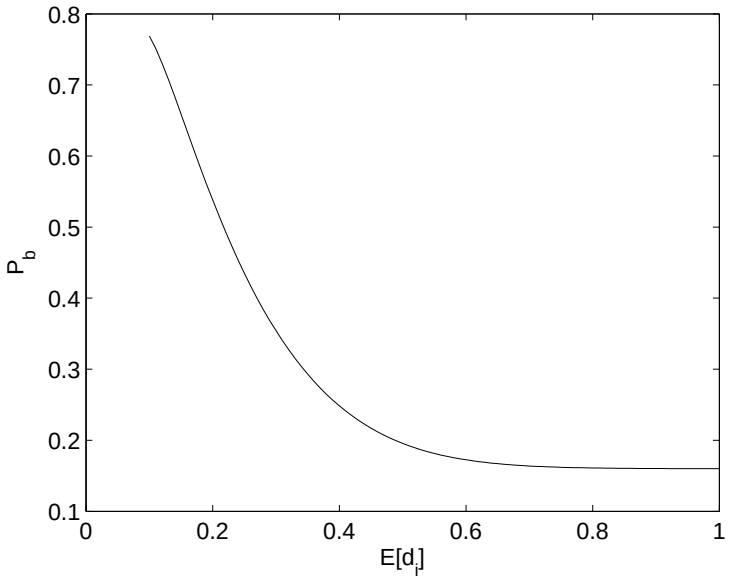

Figure 4.6: The effect of expected value of d_i to the channel performance with $r_k = 0.8$.

4.2 Channel Delay

Before exciting an impulse at the output neuron in response to an input, each impulse is subject to delay in time. The delay is found using Figure 2.4 and random diffusion

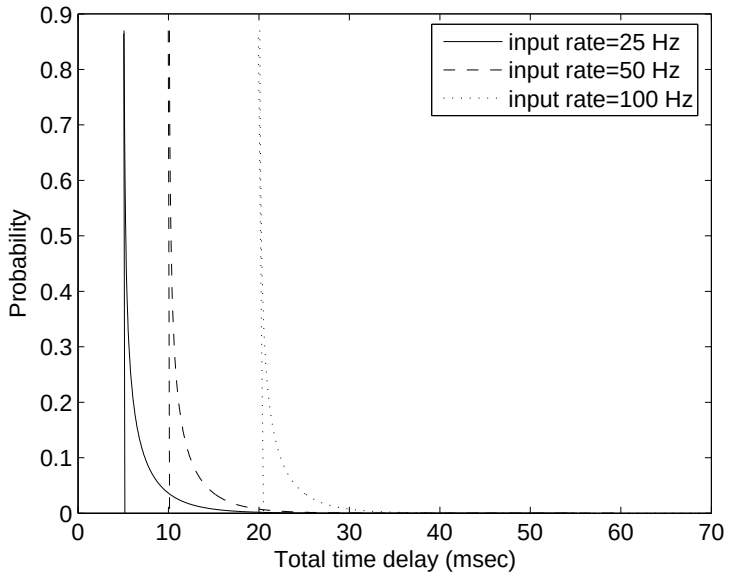

Figure 4.7: Probability density function of total time delay.

time whose probability density function is illustrated in (3.24) where b is taken as 1.

The channel delay is observed for different incoming input rates to the presynaptic terminal. The probability density function of total time delay for them is shown in Figure 4.7. According to that, higher input frequency leads to the rise in axonal propagation delay and hence, the total delay goes up.

CHAPTER 5

SYNAPTIC GAUSSIAN INTERFERENCE CHANNEL

Interference channels can appear in various fields. One special but vastly unexplored area is the neuro-spike communication.

To observe the effect of interference for the neuro-spike communication at CA region, we extend the model between one input and output terminal to the multi-input single output. For this case, the synaptic channel may be simultaneously used by many different presynaptic terminals to transmit the information, shown in Figure 5.1. Therefore, it is highly probable that released neurotransmitters from each presynaptic terminal cause interference.

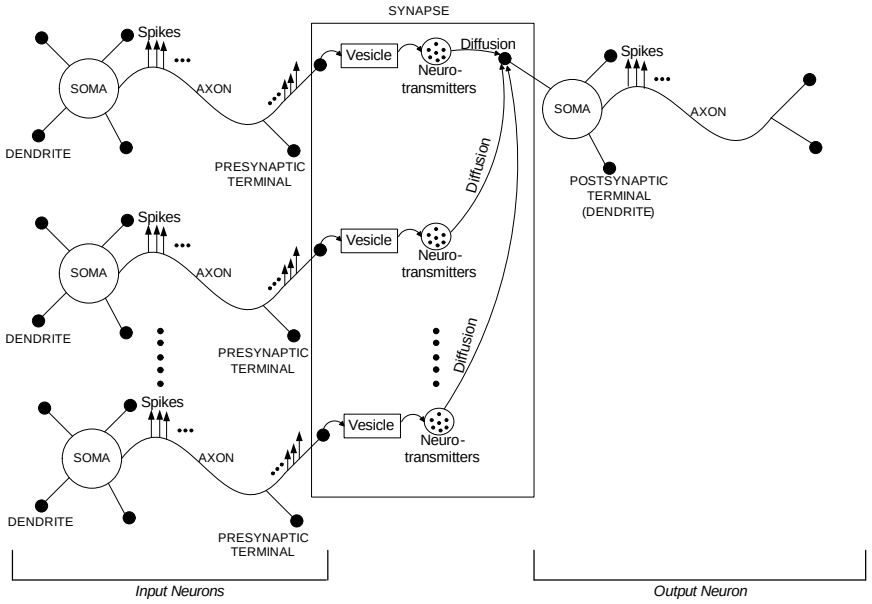

Figure 5.1: Synaptic channel.

The input spikes coming to the each presynaptic terminal have different firing rate, thus, the packet rate released to the synapse differs from one terminal to the other. In this multi-user synaptic channel, the input having low packet rate disappears among the higher ones which means loss of information. However, the cortical synapses have a gain control mechanism [30] that prevents it, which is valid for CA neurons as well [35].

A low firing rate input signal is distinguished at the output besides the stronger ones due to automatic gain control. It increases the synaptic weight of the lower rate signals automatically, hence amplifies them. The general behavior of the gain control is to adjust the synaptic weight of the inputs spontaneously in response to change in the input rate.

Realizing this principle to a Gaussian Interference Channel is an appealing idea. We define this channel as Synaptic Gaussian Interference Channel such that interference level varies according to the input strength, which may suggest enhancement in the achievable rate region of the interference channel.

The purpose of this chapter is to define a special Synaptic Gaussian Interference Channel and to characterize its achievable rate region where the interference is adjusted by the channel automatically.

5.1 Synaptic Gaussian Interference Channel

To detect the weak signal, in the channel a technique similar to the automatic gain control in synapses is applied, called Synaptic Gaussian Interference Channel. Synaptic weights are interpreted as channel gain coefficients and automatic change of them provide to distinguish weak signal at the output.

The channel is defined between $k + 1$ input terminals and single output terminal as given in Figure 5.2. Since diffusion of each neurotransmitter is Gaussian due to Green's function expressed in (2.6), the arrival process of incoming packets to the output neuron, i.e., the input distribution is Gaussian as well.

On the other hand, the channel output, y, is expressed by

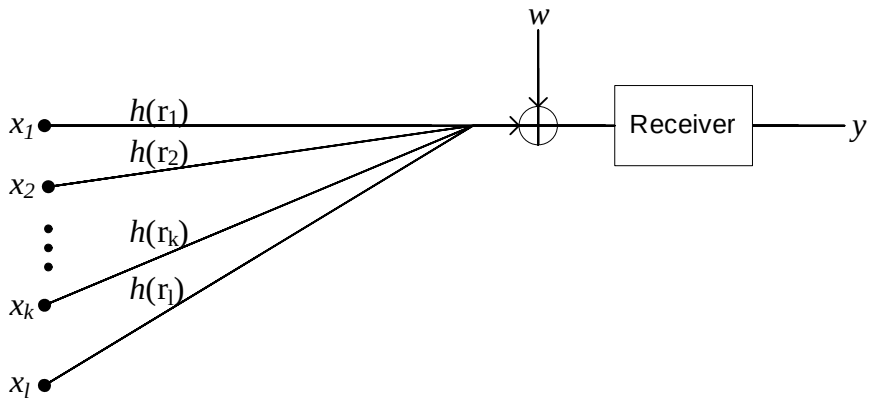

Figure 5.2: Synaptic gaussian interference channel.

$$y = \sum_{i=1}^{l} x_i |h(r_i)|^2 + w \tag{5.1}$$

where x_i denotes the input and $h(r_i)$ represents the channel gain coefficient between one input and output terminal.

w is channel noise. It is Gaussian because each packet released from one terminal is subject to sum of different type of noises. When all packets released from $k + 1$ terminals are considered, the overall noise of the channel can be taken as Gaussian in accordance with the central limit theorem.

The signal coming to the input terminal differs regarding the spike firing rate. From these $k + 1$ terminals, x_l is taken as having low firing rate and others are stronger. All inputs share the same communication medium to transmit the information.

Throughout the analysis, inputs and outputs are denoted as $x_1, x_2, \cdots, x_k, x_l$ and y respectively. The correspondent alphabets are indicated as $X_1, X_2, \cdots, X_k, X_l$ and Y.

Furthermore, we assume that each transmitter has independent and uniformly distributed message sets $m_i \in M_i = \{1, 2, \cdots, 2^{R_i}\}$ where $i \in \{1, 2, \cdots, k, l\}$. Each message, m_i, is encoded to the codeword and all codewords satisfy the power constraint such that

$$E[x_i^2] \leq P, \ \forall i \tag{5.2}$$

The encoding function, e_i, maps $e_i : m_i \rightarrow R^j$, $i \in \{1, 2, \cdots, k, l\}$.

At the output, receiver maps y to the transmitted message with d_i decoding function such that $d_i : R^j \rightarrow m_i$, $i \in \{1, 2, \cdots, k, l\}$.

5.2 Achievable Rate Region of Synaptic Gaussian Interference Channel

In this model, $k + 1$ independent senders communicate with one receiver through a common channel. This interference channel is described as

$$C = (X_1, X_2, \cdots, X_k, X_l, ; Y; S) \tag{5.3}$$

S is the conditional probability which is equal to

$$S = P(y|x_1, x_2, \cdots, x_k, x_l) \tag{5.4}$$

where $y \in Y$ and $x_1, x_2, \cdots, x_k, x_l \in (X_1, X_2, \cdots, X_k, X_l)$.

The interference channel is considered as involving two different sub-channels sharing the same medium such that the first one is in between x_l and y. The second is in between $x_1, x_2, \cdots, x_k$ and y which is a Multiple Access Channel.

The achievable rate for the first sub-channel is R_l and it is R_m for the Multiple Access Channel which is equal to

$$R_m \leq \sum_{i=1}^{k} R_i \tag{5.5}$$

Assuming all rates are the same in the Multiple Access Channel R_m determines the channel rate [34].

The rate pair (R_l, R_m) is achievable if there exists a code sequence $(2^{nR_1}, 2^{nR_2}, \cdots, 2^{nR_l}, j)$ with an average error probability which goes to zero.

We find an achievable rate pair (R_l, R_m) by dividing the interference channel into 2 sub-regions, $C1$ and $C2$ with respect to the channel gain coefficients such that

$$C1 = (X_1, X_2, \cdots, X_k, X_l; Y; S_1) \tag{5.6}$$

$$C2 = (X_1, X_2, \cdots, X_k, X_l; Y; S_2) \tag{5.7}$$

where conditional probabilities, defined in (5.4), change for different channel gain coefficients.

The approachable rate region, C is

$$C = convex\ closure\ of \bigcup_{i} Ci,\ i = 1, 2 \tag{5.8}$$

In the first region, $C1$, the square of the channel gain coefficient of x_l is greater than the sum of the others such that

$$|h(r_l)|^2 > \sum_{i=1}^{k} |h(r_i)|^2 \tag{5.9}$$

In this region, x_l is subject to the weak interference, and hence, interference is treated as noise such that

$$R_l \leq \frac{1}{2} \log(1 + \frac{|h(r_l)|^2 P_l}{N_0 + \sum_{i=1}^{k} |h(r_i)|^2 P_i}) \tag{5.10}$$

On the other hand, $x_1, x_2, \cdots, x_k$ are subject to strong interference and R_m is found as

$$R_m \leq \frac{1}{2} \log(1 + \frac{\sum_{i=1}^{k} |h(r_i)|^2 P_i}{N_0}) \tag{5.11}$$

The second region, $C2$, is opposite of the first one in terms of channel gain coefficients, i.e.,

$$|h(r_l)|^2 < \sum_{i=1}^{k} |h(r_i)|^2 \tag{5.12}$$

x_l is subject to the strong interference for this case and R_l is

$$R_l \leq \frac{1}{2} \log(1 + \frac{|h(r_l)|^2 P_l}{N_0}) \tag{5.13}$$

Conversely, $x_1, x_2, \cdots, x_k$ are subject to weak interference and R_m is found treating the interference as noise such that

$$R_m \leq \frac{1}{2} \log(1 + \frac{\sum_{i=1}^{k} |h(r_i)|^2 P_i}{N_0 + |h(r_l)|^2 P_l}) \tag{5.14}$$

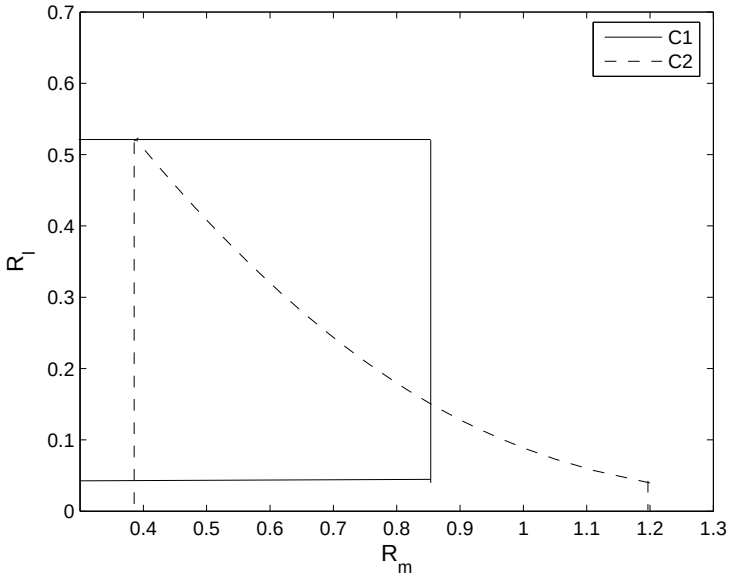

Figure 5.3: Achievable rate region for $P_l = 1, P_i = 5$.

5.3 Analysis

The achievable rate region is specified according to R_l and R_m. While doing that, N_0 is ignored, because the main synaptic noise is due to the background synaptic activity [17] stemming from the other undesired inputs.

In the analysis, the actual values of channel gain coefficients are not important. The critical point is the ratio of low signal coefficient to the others.

The achievable rate region, convex closure of $C1$ and $C2$, is shown in Figure 5.3, 5.4, 5.5, 5.6 for different P_l and P_i $\{i = 1, \cdots, k\}$ without gain control. The power of stronger inputs are all the same, because the rates for stronger inputs are considered the same at the beginning.

The increase in power for stronger inputs leads to decrease in the R_l, and hence, the achievable rate region shrinks. Likewise the power, the firing rate of stronger inputs cause a decrease in the rate region where higher power means higher firing rate.

When the power of stronger inputs are much greater than the weaker one R_l tends to 0 and achievable rate region becomes much smaller as illustrated in Figure 5.7 if the

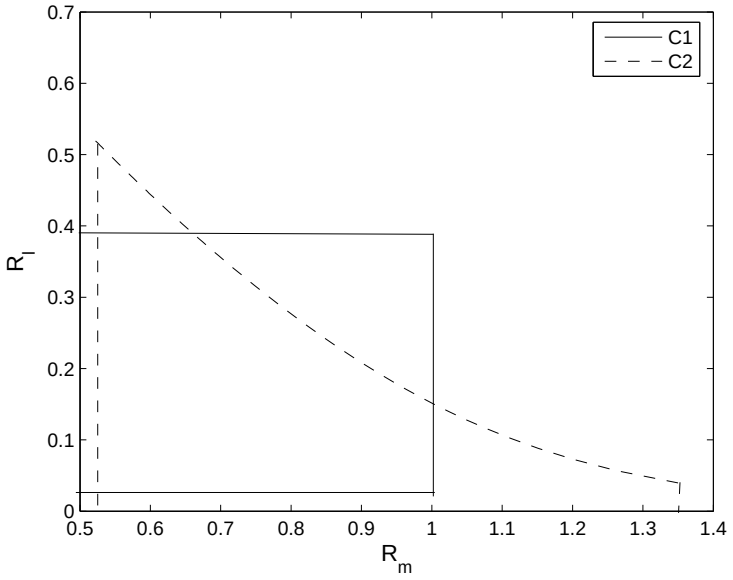

Figure 5.4: Achievable rate region for $P_l = 1, P_i = 10$.

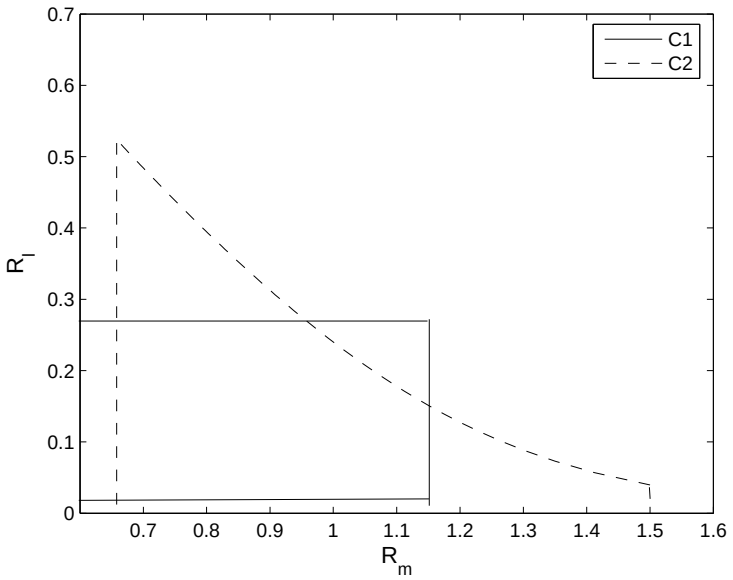

Figure 5.5: Achievable rate region for $P_l = 1, P_i = 20$.

gain control mechanism does not exist.

The gain control prevents the decrease in the achievable rate region. It increases the region in favor of lower rate signal. The reason behind the increase in the achievable rate region can be explained by decrease in the error probability while detecting the

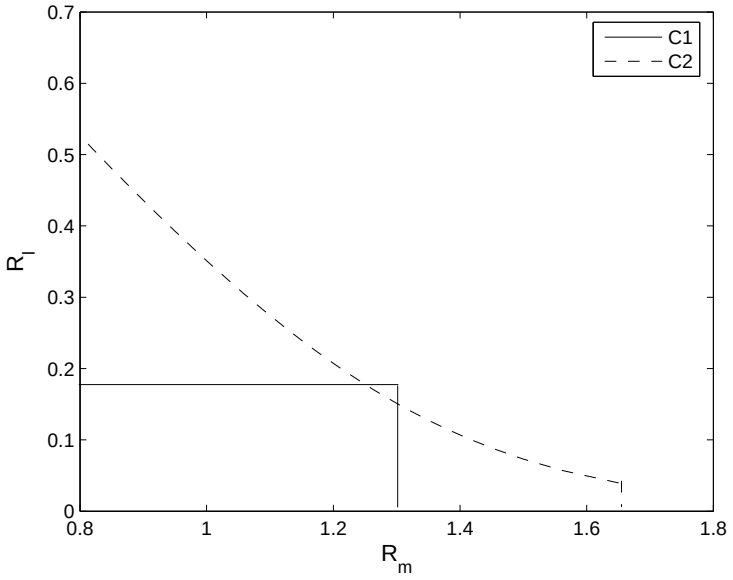

Figure 5.6: Achievable rate region for $P_l = 1, P_i = 40$.

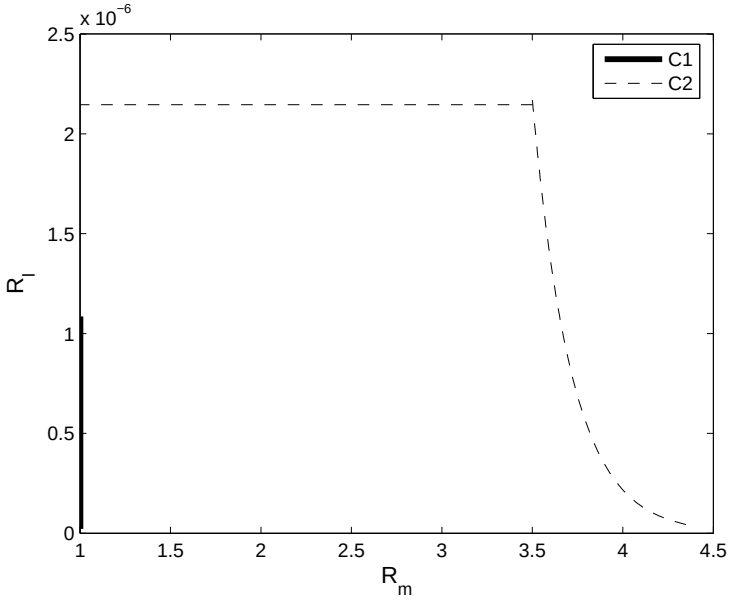

Figure 5.7: Achievable rate region for $P_l << P_i$.

weaker input spikes at the output.

The error probability of transmitting spikes from one input terminal to the single output terminal without gain control for CA neurons is found . We extend this result to $k + 1$ input terminals and one output terminal under automatic gain control mech-

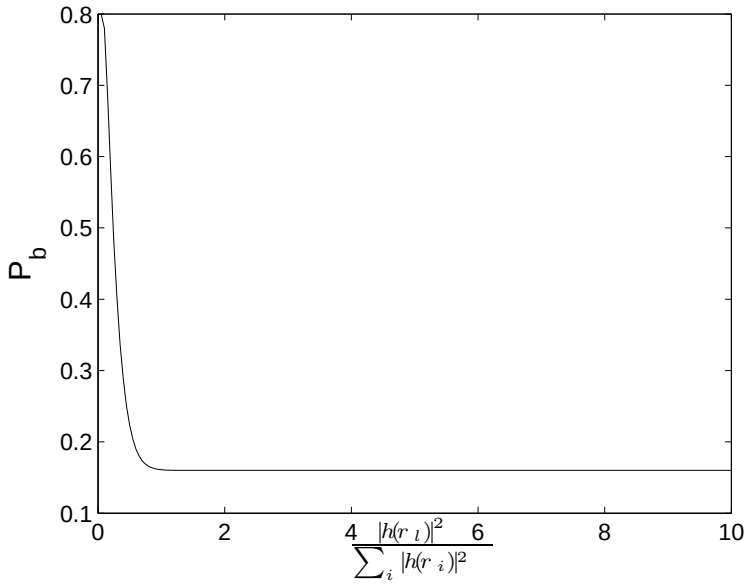

Figure 5.8: The error probability of detecting single spike.

anism. The default parameters are chosen as assigned in Table 4.1 with 0.8 release probability. The results show that depending on increase in the ratio of square of lower input coefficient to the other gain coefficients, the error probability, P_b, decreases as illustrated in Figure 5.8.

Due to automatic gain control, achievable rate region is held constant irrespective of power or firing rate of stronger inputs. This results proves that the increase in the power, firing rate and number of stronger terminals do not affect the achievable rate region, because they are compansated by the channel gain coefficients. Thus, the relation between power and channel gain coefficients can be inferred in (5.10), (5.11), (5.13), (5.14) such that

$$h(r_i) \propto \sqrt{power} \tag{5.15}$$

and

$$h(r_i) \propto \sqrt{firing\ rate} \tag{5.16}$$

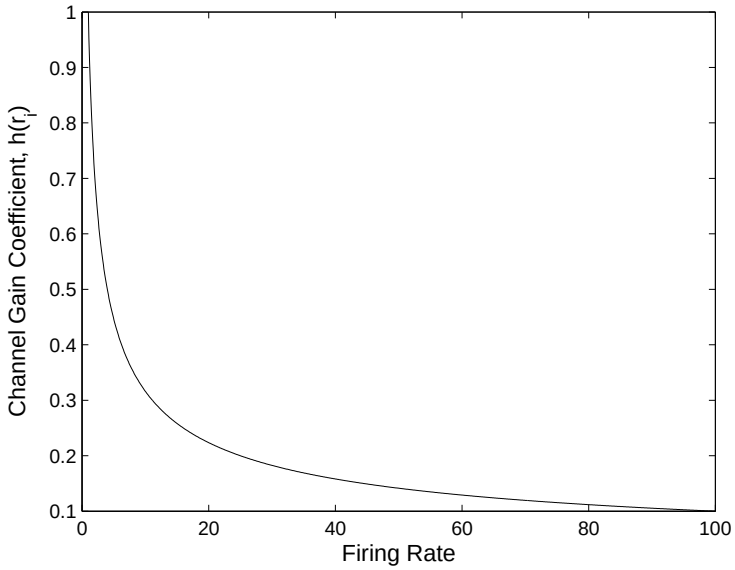

Figure 5.9: The relation between channel gain coefficient and firing rate.

This relation is observed in Figure 5.9. The same result is experimentally obtained in [30].

CHAPTER 6

CONCLUSIONS AND FUTURE WORK

The properties of the neuro-spike communication are quite different than the traditional communication and it seems efficient in terms of

- The input impulses can be transferred to the output without attenuation.
- Information is transmitted from one region to the other within short time.
- Channel quality may increase depending on high usage.

Regarding these, it is worthwhile to investigate neuro-spike communication. However, a lot of study and design paradigms are needed to set forth a complete understanding of it.

In this work, our method is to interpret the experimental results of physiological properties of neurons in terms of communication theory perspective. Therefore, we divide the neuro-spike communication into blocks according to their physiological behaviors and then, express each block regarding the communication theory.

For this purpose, firstly, neuro-spike channel between one input and output neuron at CA region is modeled. We propose that this realistic model can be used as a new bio-inspired physical channel for nanonetworks.

Secondly, the analysis of the channel model is performed. The analysis reveals that an efficient communication can be obtained for low incoming signal rate to the presynaptic terminal, higher number of NMDA receptors at the output and low synaptic noise. Moreover, having smaller threshold value, greater alpha functions for both

AMPA and NMDA, and higher expected value of the random amplitude distortion contribute to the channel performance. Furthermore, input frequency must be lower to have a smaller time delay.

Lastly, the model between one input and output terminal is extended to multi-input, single output case in order to observe the effect of interference at synapses. We define a special Gaussian Interference Channel such that the transmission rate regime alters according to the channel gain coefficients. These coefficients are adjusted in compatible with the incoming signal rate automatically. This technique, similar to the neural behavior, provides one solution to reduce the effect of the interference for Gaussian Interference Channel.

Moreover, the achievable rate region of Synaptic Gaussian Interference Channel is characterized in terms of power or firing rate. It is shown that the weaker signal is not affected negatively to the increase in the power of others because of gain control structure. Moreover, gain control improves the probability of transmitting single spike correctly to the output for multiple input channel. Hence, the channel capacity is enhanced.

Our ongoing works are to develop appropriate protocols for the modeled channel between two neurons in order to realize a complete artificial neuro-inspired nanonetwork architecture. In addition to that, the Synaptic Gaussian Interference Channel can be extended from single output to multi-output terminal as a future work and the enhancement in the channel capacity can be observed for that channel. Furthermore, the results of this multi-input, multi-output communication can be utilized when hopping presents in the channel, i.e., large numbers of terminals are participated to the communication. This leads to the complete characterization of the neural communication capacity.

REFERENCES

[1] I. F. Akyildiz, F. Brunetti, C. Blazquez, "NanoNetworking: A New Communication Paradigm," *Computer Networks Journal (Elsevier)*, June 2008.

[2] J. M. Bekkers, G. B. Richerson, C. F. Stevens, "Origin of Variability in Quanta1 Size in Cultured Hippocampal Neurons and Hippocampal Slices," *Proc. Natl. Acad Sci. USA*, vol. 87, pp. 5359-5362, July 1990.

[3] J. M. Bekkers, C. F. Stevens, "Quantal Analysis of EPSCs Recorded from Small Numbers of Synapses in Hippocampal Cultures," *Journal of Neurophysiology*, 73(3), 1145-1156, Mar. 1995.

[4] T. V. P. Bliss, G. L. Collingridge, "A synaptic model of memory: long-term potentiation in the hippocampus," *Nature*, vol. 361, Jan. 1993.

[5] P. Dayan, L. F. Abbott, "Neuroscience: Computational and Mathematical Modeling of Neural Systems," *Cambridge, MA:MIT Press*, 2001.

[6] L. J. DeFelice, "Introduction to Membrane Noise," *Plenum Press: New York*, 1981.

[7] L. E. Dobrunz, C. F. Stevens, "Heterogeneity of release probability, facilitation, and depletion at central synapses," *Neuron*, vol. 18, pp. 995-1008, June 1997.

[8] A. Enomoto, M. Moore, T. Nakano, et al., "A molecular communication system using a network of cytoskeletal filaments," *in: Proceedings of the 2006 NSTI Nanotechnology Conference*, May 2006.

[9] A. A. Faisal, S. B. Laughlin, "Stochastic simulations on the reliability of action potential propagation in thin axons," *PLoS Computational Biology*, vol. 3, Issue. 5, e79, May 2007.

[10] A. A. Faisal, L. P. J. Selen, D. M. Wolpert, "Noise in the nervous system," *Nature*, vol. 9, Apr. 2008.

[11] L. R. Squire, J. L. Roberts, N. C. Spitzer, M. J. Zigmond, S. K. McConnell, F. E. Bloom, "Fundamental Neuroscience," *Boston : Academic Press*, 2008.

[12] L. P. Gine, I. F. Akyildiz, "Molecular communication options for long range nanonetworks," *Computer Networks (Elsevier)*, vol. 53, no. 16, pp. 2753-2766, Nov. 2009.

[13] A. J. Goldsmith, P. P. Varaiya, "Capacity, Mutual Information, and Coding for Finite-State Markov Channels," *IEEE Trans. Inform. Theory*, vol. 42, pp. 868-886, May 1996.

[14] A. Guney, "Mobile Ad Hoc Molecular Nanonetworks," *M.S. thesis, Middle East Technical University*, 2010.

[15] A. Guney, B. Atakan, O. B. Akan, "Mobile Ad Hoc Nanonetworks with Collision-based Molecular Communication," submitted for publication, 2010.

[16] S. Hiyama, Y. Moritani, T. Suda, R. Egashira, A. Enomoto, M. Moore, T. Nakano, "Molecular communication," *in: Proceedings of the NSTI Nanotechnology Conference*, Oct. 2005.

[17] A. Manwani, "Information-theoretic Analysis of Neuronal Communication," *Ph.D. dissertation, California Institute of Technology, California*, 2000.

[18] H. Markram, J. Lubke, M. Frotscher, A. Roth, B. Sakmann, "Physiology and anatomy of synaptic connections between thick tufted pyramidal neurones in the developing rat neocortex," *Journal of Physiology*, 500.2, pp. 409-440, 1997.

[19] J. P. Meeks, S. Mennerick, "Action Potential Initiation and Propagation in CA3 Pyramidal Axons," *Journal of Neurophysiology*, vol. 97, pp. 3460-3472, May 2007.

[20] M. Pierobon, I. F. Akyildiz, "A physical channel model for molecular communication in nanonetworks," *IEEE Journal on Selected Areas in Communication*, vol. 28, no. 4, May 2010.

[21] M. Raastad, G. M. G. Shepherd, "Single axon action potentials in the rat hippocampal cortex," *The Journal of Physiology*, 548.3, pp. 745-752, 2003.

[22] W. Rall, "Distinguishing theoretical synaptic potentials computed for different some-dendritic distributions of synaptic inputs," *Journal of Neurophysiology*, 30, pp. 1138-1168, 1967.

[23] J. B. Jr. Ranck, "Studies on single neurons in dorsal hippocampal formation and septum in unrestrained rats. I. Behavioral correlates and firing repertoires," *Experimental Neurology*, 41(2), 462-531, 1973.

[24] T. Schikorski, C. F. Stevens, "Quantitative ultrastructural analysis of hippocampal excitatory synapses," *The Journal of Neuroscience*, 17(15):5858-5867, Aug. 1997.

[25] D. L. Snyder, "Random Point Processes," *New York: Wiley*, Nov. 1975.

[26] C. F. Stevens, Y. Wang, "Facilitation and depression at single central synapses," *Neuron 14*, vol. 14, pp. 795-802, Apr. 1995.

[27] H. S. Wang, N. Moayeri, "Finite-State Markov Channel-A Useful Model for Radio Communication Channels," *Transactions on Vehicular Technology*, vol. 44, no. 1, 1995.

[28] A. Wong, B. Graham, B. Billups, I. Forsythe, "Distinguishing between presynaptic and postsynaptic mechanisms of short-term depression during action potential trains," *Journal of Neuroscience*, 23, 4868-4877, 2003.

[29] Z. Yang, M. H. Hennig, "Wide-band information transmission at the calyx of Held," *Neural Computation*, 21(4), 991-1017, Apr. 2009.

[30] L. F. Abbott, J. A. Varela, K. Sen, S. B. Nelson, "Synaptic Depression and Cortical Gain Control," *Science*, vol. 275, Jan. 1997.

[31] A. B. Carleial, "A case where intereference does not reduce capacity," *IEEE Trans. Inform. Theory*, vol. IT-21, pp. 569-570, Sept. 1975.

[32] H. Sato, "The capacity of the gaussian interference channel under strong interference," *IEEE Trans. Inform. Theory*, vol. IT-27, pp. 786-788, Nov. 1981.

[33] T. S. Han, K. Kobayashi, "A new achievable rate region for the interference channel," *IEEE Trans. Inform. Theory*, vol. IT-27, pp. 49-60, Jan. 1981.

[34] T. M. Cover, J. A. Thomas, "Elements of information theory," *Wiley-Interscience*, 2006.

[35] A. Kirkwood, S. M. Dudek, J. T. Gold, C. D. Aizenman, M. F. Bear, "Common forms of synaptic plasticity in the hippocampus and neocortex in vitro," *Science*, vol. 260, June 1993.

APPENDIX A

DERIVATION OF MEAN AND AUTOCORRELATION FUNCTION OF DOUBLY STOCHASTIC POISSON PROCESS

N(t) is a doubly stochastic poisson process with integrable, non-negative λ_n random stationary intensity function. Its mean value is

$$E[N(t)] = \sum_{n=0}^{\infty} nP(N(t) = n) \tag{A.1}$$

We define an auxiliary parameter such that

$$\eta = \int_{t}^{t_x} \lambda_n d_n \tag{A.2}$$

Similar to [25]

$$P(N(t) = n) = E[P(N(t) = n/\eta)] \tag{A.3}$$

(A.1) becomes

$$E[N(t)] = \sum_{n=0}^{\infty} nE[\frac{\eta^n exp(-\eta)}{n!}] \tag{A.4}$$

$n - 1$ is assigned to m. Hence,

$$E[N(t)] = E[\eta \sum_{m=0}^{\infty} (\frac{\eta^m exp(-\eta)}{m!})] \tag{A.5}$$

Therefore,

$$E[N(t)] = E[\eta] \tag{A.6}$$

The autocorrelation function of the N(t) is

$$R_{N(t_1,t_2)} = E[N(t_1)N(t_2)] \tag{A.7}$$

$t_2 = t_1 + t$, and

$$E[N(t_1)N(t_2)] = \sum_{n_1=0}^{\infty} n_1 P(N(t) = n_1) \sum_{n_2=0}^{\infty} n_2 P(N(t) = n_2) \tag{A.8}$$

where

$$P(N(t) = n_1) = E[P(N(t) = n_1/\eta_1)] \tag{A.9}$$

$$P(N(t) = n_2) = E[P(N(t) = n_2/\eta_2)] \tag{A.10}$$

with the following η_1 and η_2

$$\eta_1 = \int_{t_1}^{t_x} \lambda_n d_n \tag{A.11}$$

$$\eta_2 = \int_{t_2}^{t_x} \lambda_n d_n \tag{A.12}$$

Similarly,

$$R_{N(t_1,t_2)} = E[\eta_1 \eta_2] \tag{A.13}$$

Since λ_n is a random stationary function,

$$R_{N(t)} = E[\eta_1 \eta_2] \tag{A.14}$$

APPENDIX B

CONDITIONAL MUTUAL INFORMATION DERIVATION FOR PACKET RELEASED MECHANISM

From Markovian state transition property, (3.67) can be written as

$$\rho_n = P(s_n|x^{n-1}, s_{n-1}) \tag{B.1}$$

Due to chain rule

$$I(q^n; x^n|\gamma = \Gamma) = \sum_{i=1}^{n} H(x_i|x^{i-1}, \gamma = \Gamma) - \sum_{i=1}^{n} H(x_i|x^{i-1}, q^i, \gamma = \Gamma) \tag{B.2}$$

To obtain the first term of RHS in (B.2)

$$H(x_i|x^{i-1}, \gamma = \Gamma) = \sum_{x^{i-1}} p(x^{i-1}) H(x_i|x^{i-1} = x^{i-1}, \gamma = \Gamma) \tag{B.3}$$

where

$$H(x_i|x^{i-1} = x^{i-1}, \gamma = \Gamma) = -\sum_{x_i} p(x_i|x^{i-1}, \gamma) \log p(x_i|x^{i-1}, \gamma) \tag{B.4}$$

Using the results in [13], when the FSMC transition structure is known, $p(x_i|x^{i-1}, \gamma)$ can be expressed by

$$p(x_i|x^{i-1}, \gamma) = \sum_{m} p(x_i|s_i = s_m, \gamma) \sum_{l} p(s_i = s_m|x^{i-1}, s_{i-1} = s_l) \tag{B.5}$$

Since $\sum_l p(s_i = s_m|x^{i-1}, s_{i-1} = s_l) = \sum_l \rho_{i(lm)}$, (B.5) reduces to

$$p(x_i|x^{i-1}, \gamma) = \sum_{m} p(x_i|s_i = s_m, \gamma) \sum_{l} \rho_{i(lm)} \tag{B.6}$$

The RHS of (B.6) is simplified to

$$p(x_i|x^{i-1}, \gamma) = \sum_{l} p(x_i|\rho_{i(l)}, \gamma) = p(x_i|\rho_i, \gamma) \tag{B.7}$$

Hence, the conditional entropy belonging in (B.3) is

$$H(x_i|x^{i-1}, \gamma = \Gamma) = H(x_i|\rho_i, \gamma = \Gamma) \tag{B.8}$$

Since ρ_n is independent from the input, it can be written as

$$\rho_n = P(s_n|x^{n-1}, s_{n-1}, q^{n-1}) \tag{B.9}$$

To obtain the second term of RHS in (B.2)

$$H(x_i|x^{i-1}, q^i, \gamma = \Gamma) = \sum_{x^{i-1}} p(x^{i-1}) \sum_{q^i} p(q^i) H(x_i|x^{i-1} = x^{i-1}, q^i = q^i, \gamma = \Gamma) \tag{B.10}$$

where

$$H(x_i|x^{i-1} = x^{i-1}, q^i = q^i, \gamma = \Gamma) = -\sum_{x^i} p(x_i|x^{i-1}, q^i, \gamma) \log p(x_i|x^{i-1}, q^i, \gamma) \tag{B.11}$$

Similar to the above procedure, $p(x_i|x^{i-1}, q^i, \gamma)$ can be simplified to

$$p(x_i|x^{i-1}, q^i, \gamma) = p(x_i|q^i, \rho_i, \gamma) \tag{B.12}$$

Hence, the conditional entropy in (B.10) is

$$H(x_i|x^{i-1}, q^i, \gamma = \Gamma) = H(x_i|q^i, \rho_i, \gamma) \tag{B.13}$$

From (B.8) and (B.13)

$$I(q^n; x^n|\gamma) = \sum_{i=1}^{n} [H(x^i|\rho_i, \gamma) - H(x^i|q^i, \rho_i, \gamma)] \tag{B.14}$$